BOEING

D256-10202

UNDERCOOLING OF MATERIALS DURING SOLIDIFICATION IN SPACE

FINAL REPORT

CONTRACT NAS8-31238
(1-5-58-00217 1F)

AUGUST 31, 1976

Prepared by

THE NUCLEAR AND SPACE PHYSICS DEPARTMENT
BOEING AEROSPACE COMPANY
P. O. Box 1470
HUNTSVILLE, ALABAMA 35807

R. I. MILLER - PRINCIPAL INVESTIGATOR

R. R. BROWN - PROGRAM MANAGER

Prepared for

NATIONAL AERONAUTICS AND SPACE ADMINISTRATION
GEORGE C. MARSHALL SPACE FLIGHT CENTER
MARSHALL SPACE FLIGHT CENTER, ALABAMA

ABSTRACT

This document describes a theoretical research program on the undercooling and solidification of materials under variable external field conditions performed by The Boeing Aerospace Company for the National Aeronautics and Space Administration. Work was performed under the direction of Dr. Mary Helen Johnston of Marshall Space Flight Center, the Contracting Officer's Representative.

A catalog of theories and models of nucleation of solid phases in the melt is provided in the document, as is discussion of the relation of undercooling to intermolecular potentials, the dependence of growth rate on undercooling, the influence of undercooling on liquid-solid interface stability and solid structure, the direct effects of external fields on melts, the relation of solid physical properties to structure and the role of nucleants in solidification. Results of theoretical analysis of several experiments related to the Space Processing Applications Program are given in the document, and recommendations for future experiments and further theoretical development along with procedures for correlation of theory and experiment are specified for solidification in space research.

TABLE OF CONTENTS

TABLE OF CONTENTS (Continued)

LIST OF FIGURES

LIST OF FIGURES (Continued)

LIST OF TABLES

LIST OF COMMONLY USED SYMBOLS

A	- Product of terms in exponent of nucleation rate equation
A_i	- Various constants or areas
a or a_o	- Lattice molecule dimension or lattice parameter
a^*	- Critical dimension, a
Δa	- Difference in a between nucleus and substrate
B, B_i	- Various constants
b or b_o	- Molecule dimension in a lattice or lattice parameter
b^*	- Critical dimension, b
C, C_i	- Component concentration
$C_{m,n}$	- Elastic constants for a solid
C_T	- Total concentration or number density
c or c_p	- Specific heat
c or c_o	- Molecule dimension in a lattice or lattice parameter
c^*	- Critical dimension, c
D	- Diffusion coefficient
e	- Base of natural logarithms, 2.71828 ... - Charge of an electron, 1.6×10^{-19} coulomb
F	- Helmholtz free energy
$f(\theta)$	- Heterogeneous nucleation or wetting angle function, $\frac{1}{4}(2 + \cos\theta)(1 - \cos\theta)^2$
$f(z)$	- Function of z

LIST OF COMMONLY USED SYMBOLS (Continued)

G	- Gibbs free energy or modulus of rigidity
ΔG	- Change in Gibbs free energy corresponding to a state change
ΔG_D	- Free energy barrier for diffusion
ΔG^*	- Critical free energy for nucleus formation
ΔG_V	- Free energy per unit volume
g	- Acceleration due to gravity or simulated gravity
δg	- Change in g from 980 cm/sec^2
H	- Magnitude of magnetic field strength
H_o	- Magnetic field in a material-free region
h	- Planck's constant, 6.6253×10^{-27} erg sec
	- Cylindrical height
$\hbar$	- $h/2\pi$
h^*	- Critical value of height, h
I	- Nucleation rate
	- Moment of inertia
I_o	- Pre-exponential in nucleation rate equation, often taken to be 10^{33} $nuclei/cm^3sec$
K	- Curvature of a liquid solid interface
K_i	- Various constants
k	- Boltzmann's constant, 1.3804×10^{-16} erg/deg
	- Solute distribution coefficient, C_S/C_L
ℓ	- Dendrite spacing or grain size, $(\frac{V}{N})^{1/3}$

LIST OF COMMONLY USED SYMBOLS (Continued)

M	- Atomic weight - Nucleus mass - Product of constants in solidification model
m	- Liquidus slope - Atomic or molecular mass - Counting index
N	- Total number of nuclei, atoms, molecules, etc. in a system
N_o	- Avogadro's number, $6.025 \times 10^{+23}$ $mole^{-1}$
n	- Number of moles - Number density - Counting index
p, p_i	- Momentum
Q	- Heat of fusion - Canonical ensemble partition function
Q'	- Thermoelectric power
q	- Generalized coordinate
q_r	- Rotational partition function
q_{rep}	- Replacement partition function
q_t	- Translational partition function
R	- Base radius of a spherical cap radius
r	- Spherical or cylindrical radius
r_i, r_{ij}	- Generalized coordinate
r^*	- Radius of a critical nucleus

LIST OF COMMONLY USED SYMBOLS (Continued)

S_c	- Entropy of fusion, $\frac{Q}{T_M}$
T	- Temperature
T_m	- Equilibrium melting (freezing) temperature
ΔT	- Undercooling, $T_M - T$
δT	- Change in temperature directly due to change in external field conditions
t	- Time
δt_d	- Maximum time for solute molecule diffusion
δt_h	- Maximum time for heat flow
U	- Nucleus velocity in a melt
U_c	- Solid growth rate
u	- Molecular or atomic velocity in a melt
V	- Total material system volume or velocity of a gross liquid-solid interface into a melt
V_V	- Volume fraction (metallographic)
v or υ	- Specific volume
v_d	- Dendrite volume
v_g	- Volume of a dendrite due to growth
v_n	- Volume of a dendrite due to nucleation
δv	- Change in volume due to external field effects
X	- Solute atomic fraction
x	- Position coordinate

LIST OF COMMONLY USED SYMBOLS (Continued)

y	- Generalized material property
Z	- Grand canonical ensemble partition function
z	- Axial coordinate or vertical distance
α	- Thermal expansion coefficient or counting index
α, α_T	- Thermal diffusivity
β	- Isothermal compressibility or counting index
γ	- $\frac{M}{2kT}$ in Section 2.2.4 or counting index
γ_j	- Magnitude of interfacial tension
	- Various constants
δ	- $\frac{\Delta a}{a_o}$ in Section 2.1.3
	- Interface perturbation amplitude in Section 2.2.3
ϵ	- Grain boundary orientation angle
η	- Viscosity
θ	- Wetting angle, other angles
κ	- Thermal conductivity
Λ	- Phonon mean free path
λ	- Thermal wavelength, $\sqrt{\frac{h^2}{2\pi mkT}}$
	- Perturbation wavelength or lamellar dimension

LIST OF COMMONLY USED SYMBOLS (Continued)

μ	- Chemical potential
μ_o	- Magnetic permeability of free space
$\Delta\mu_V$	- Change in μ per unit volume = $\Delta G_V = S_c \Delta T$
ν	- Poisson's ratio
ξ	- Negligibly small value of nucleation rate corresponding to maximum undercooling
π	- 3.14159...
ρ	- Density
ρ_e	- Electrical resistivity
Σ	- Summation symbol
σ, σ_i	- General liquid-solid interfacial energy
σ_{nl}	- Energy of the nucleus-liquid interface
σ_{sn}	- Energy of the substrate-nucleus interface
σ_{sl}	- Energy of the substrate-liquid interface
σ_e	- Electrical conductivity
$\Delta\sigma$	- $\frac{1}{2}\ \sigma_{nl}\ (1 - \cos\theta)$
ϕ	- Intermolecular potential energy
ϕ_i	- Nearest neighbor interaction energy corresponding to the i^{th} face of a nucleus, Section 2.1.3

LIST OF COMMONLY USED SYMBOLS (Concluded)

χ	- Magnetic susceptibility
ω	- Frequency, $\frac{2\pi}{\lambda}$
ω_i	- Interatomic or intermolecular vibration frequencies
∂	- Partial derivative symbol
$\vec{\nabla}$	- Vector partial differential operator, del
∇^2	- $\vec{\nabla}\cdot\vec{\nabla}$
$\int$	- Integral symbol

PART 1 - SUMMARY

1.1 STUDY OBJECTIVES

It is commonly accepted in science and engineering that a phenomenon is not really understood until a mathematical theory of the phenomenon is developed from which quantitative predictions can be made which agree with experimental studies of the phenomenon. Thus the over-all purpose of the study "Undercooling of Materials During Solidification in Space" is to theoretically determine how undercooling, gravity and nucleants affect the solidification of materials from the melt and influence the properties of the resultant solid. Specific objectives which complement this purpose include:

1. Gain an understanding of the theoretical relationship between undercooling and both homogeneous and heterogeneous nucleation.

2. Determine the influence of external fields (particularly gravity) on the nucleation process.

3. Gain an understanding of how solidification history affects the physical properties of a material.

4. Theoretically analyze some solidification experiments performed at MSFC and as part of the Space Processing Applications Rocket (SPAR) program.

5. Specify materials to be used in the comparison of theory to experiments in one-g and zero-g.

The twelve-month research program described by this report constitutes a major step toward achieving these ambitious objectives.

1.2 APPROACH

The basic approach to this study was to obtain knowledge of the theory of nucleation from the melt (nucleation of solid or liquid phases in a vapor phase was not considered), and adapt the theory to Space Processing program needs and experiments in which the acceleration due to gravity, g, is a variable. In cases where Space Processing experimental situations did not correspond to existing theory, original theoretical relationships were developed to carry out the required analyses.

The above approach was organized around four tasks:

1. Evaluation of Nucleation Theories

2. Influence of Undercooling and Nucleation on Properties of Solids

3. Investigation of Field Effects on Undercooling and Nucleation

4. Correlation of Theoretical and Experimental Results

The theories and models identified in Task 1 were used in Tasks 2, 3 and 4 to explore previously unanalyzed experimental results, and to begin development of a theoretical model to predict solid material properties from the melt properties and the solidification environment. Environmental variables considered include gravity level, nucleants (impurities, particles of high temperature phases and container surfaces) and temperature (undercooling).

Theories and models of nucleation from the melt were obtained from the literature, and included both classical and modern homogeneous nucleation theories, heterogeneous nucleation theories and models and energetic aspects of nucleation in two-component melts. Most of classical nucleation theory is based on the work of David Turnbull. His experimental and theoretical results form the basis for much of this study (see References). These theories were used to derive equations which show how undercooling

1.2 (Continued)

influences liquid-solid interface stability, growth rate, nucleation rate and structure of material solidified from the melt. An approach to relating solid physical properties to structure was developed for use in the comprehensive model for solid property prediction. Other theoretical research included: an explanation of why some pure materials sustain higher undercooling (before homogeneous nucleation initiates) and others; how nuclei segregate in a melt under the influence of acceleration fields; the direct effects of external fields on solidification; and some mathematical analysis of experiments performed at MSFC, in SPAR flights, and experiments performed by Kattamis, et.al., which are applicable to Space Processing goals.

1.3 RESULTS OF THE STUDY

Nucleation Theory

A catalog of theories of nucleation from the melt has been created (see Section 2.1), containing the theories of classical and modern homogeneous nucleation, heterogeneous nucleation and nucleation in two-component melts. For both homogeneous and heterogeneous nucleation, models are given which describe the formation of nuclei of different shapes. The most common case, heterogeneous nucleation, is most easily described in terms of a spherical cap shaped nucleus and the angle the tangent to this cap nucleus makes with the nucleant surface, called the wetting angle, θ. This angle is related to the interfacial energies between nucleus and melt, nucleus and nucleant and nucleant and melt. Other parameters related to these same interfacial energies are derived for different nucleus shapes, but since the exact shape of a nucleus is seldom known, θ provides a convenient parameter for characterizing this aspect of nucleation. Nucleants considered included particles of high temperature phases suspended in the melt as well as other impurities which might be present, and melt container surfaces. A major question in nucleation theory, which remains unanswered as yet, is the exact mechanism by which a particular

1.3 (Continued)

nucleant causes a nucleus to form. Research reported in the literature centers on disregistry between the lattice structure of the nucleant and that of the nucleus, but there is no agreement among authors as to what the mechanism involved is or how to describe it theoretically.

Maximum Undercooling

The question of why two different pure materials, with no nucleants present, will homogeneously nucleate at different undercoolings has been resolved by showing that the maximum undercooling a pure melt can attain is proportional to the ratio $\sigma^{3/2}/S_c$ where σ is the liquid-solid interfacial energy and S_c is the entropy of fusion for the material (see Section 2.2.1). S_c is related to the intermolecular potentials of both the liquid and solid phases by statistical mechanics. σ can be related to liquid or solid phase intermolecular potentials by several semi-empirical theories, most of which involve structural models of the liquid-solid interface. Thus the maximum undercooling attainable in a pure melt is a (complicated) function of the intermolecular potentials of the material, and hence is a unique characteristic of that material.

Environmental Effects on Nuclei

Experiments by Dr. Johnston at MSFC have shown a pronounced solute segregation effect in lead-tin eutectic material as a function of the environmental variables gravity level (acceleration) and undercooling (temperature). Although an increase in segregation with gravity level was expected, a segregation increase with increasing undercooling was not. To analyze this situation, it was assumed that nuclei settle in the melt due to gravity, and segregate further due to an unexplained undercooling effect which may or may not be coupled to the gravity effect. The gravity effect was analyzed by solving the equation of motion for a nucleus moving in the melt and substituting

1.3 (Continued)

the result into Fick's law for concentration distribution in the melt (see Section 2.2.4). The resulting differential equation can be solved, yielding a transcendental equation for solute concentration as a function of position in the melt, gravity and undercooling. This equation is in good agreement with experimental (one-g) concentration distribution data reported in the literature. It also shows qualitative agreement with the MSFC experiment for concentration versus gravity level, if allowance is made for the unexplained undercooling effect. There is no agreement between theory and experiment for concentration as a function of undercooling, the experimental data being approximately linear and the theoretical equation being strongly exponential. Several theoretical hypotheses for this undercooling effect were tested, but none showed agreement with the observed experimental data. Further research is needed to identify the mechanism of this anomalous undercooling effect. A paper detailing the above work was presented at the Winter Meeting of the American Physical Society, held at California Institute of Technology (Bull.Am.Phys.Soc., 20, 1511, 1975).

Solidification Model Development

As part of the over-all goal of this study to ascertain how solidification environment affects resultant solid properties, an attempt was made to develop a mathematical model which would predict grain size and dendrite volume, morphology and spacing as a function of nucleant wetting angle, θ, and the undercooling, ΔT (see Section 2.2.7). This model, in its present form, solves 8 simultaneous equations; those for nucleus volume, dendrite growth volume, dendrite growth rate, number of nuclei created, nucleation rate, nucleus critical radius, maximum solute diffusion time and maximum heat flux time. A Wang 700A computer program was written for calculations with this set of equations. The model has been compared to experimental studies by Kattamis and Flemings on iron-nickel alloy, and shows rough agreement with the experimental data over limited ranges of undercooling. But for the most part, the theory does not yet reflect

1.3 (Continued)

the experimental findings, largely because of simplifying assumptions which lead to rather unrealistic equations. A great deal of additional time and effort will be required to derive rigorous expressions for such parameters as total solidification time, dendrite growth volume and solute diffusion time. Model development thus far does, however, provide a firm basis for further research, and also provides grounds for the hope that the solidification model can be refined to give reasonably accurate predictions of grain size and dendrite volume and morphology data.

Comprehensive Property Prediction Model

Work with the solidification model has lead to the concept of the comprehensive property prediction model (CPPM) (see Section 2.4.1), which is to be composed of several elements (comprehensive refers to its multi-model composition), each of which models a different part of the solidification process. Output of the CPPM would be solid material properties calculated from input consisting of melt property (constant) data and external environmental variables, such as gravity level, nucleant wetting angle and cooling rates (which lead in the heat transfer model to undercooling values). Once the solid properties have been output, they can be compared to material property requirements specified by the potential user of the material. If calculated values are too far from the required values of material properties, new melt properties (signifying different melt components or solute concentrations) along with altered environmental variable ranges, if needed, can be input again, and this iteration repeated until a match between calculated solid properties and user requirements is obtained. In addition to its usefulness as a molecular-level materials design tool, the CPPM could be used by the Space Processing Applications (SPA) program as a guide for the definition and design of SPA experiments and as an aid in selecting the most promising material combinations (from among the 100 million or so two-to-five component

1.3 (Continued)

alloys possible in microgravity) for flight experiments. Therefore, development of a CPPM should receive emphasis within the SPA Program.

Relation of Physical Properties to Structure

One element of a potential CPPM which received attention during this study was the theoretical relationship between material structure and physical properties (see Section 2.2.6). Most solid physical properties derive from the periodic nature of the crystal lattice and its symmetry with respect to spatial operations and the electron and phonon energy spectra characteristic of the material. However, a few physical properties are influenced by non-periodic structures in the solid, such as grain boundaries, impurities or other sites of electron and phonon scattering. In particular, three physical properties of solids, the thermal conductivity, the electrical conductivity and the thermoelectric power have been found to depend on the phonon mean free path in the solid. The phonon mean free path is itself related approximately to grain size in the solid. The dependence of these properties on grain size is usually masked by the fact that thermal conductivity is proportional to heat capacity as well as phonon mean free path, and heat capacity varies much more rapidly with temperature than mean free path varies with grain size. Thus thermal conductivity, electrical conductivity and thermoelectric power are influenced by grain size in the solid, though to a lesser extent than by temperature.

SPAR Experiments

Two SPAR experiments to investigate the solidification of the metal-model material, ammonium chloride solution (NH_4Cl-H_2O), were flown during the study period (see Section 2.3.1). Certain aspects of these experiments were analyzed theoretically: the undercooling of the first sample corresponding to measured growth rates, and the failure of the second sample to solidify, even with substantial undercooling.

1.3 (Continued)

Very few of the melt property parameters for NH_4Cl-H_2O are known, so to do calculations for this material, nominal metal values (since it is a metal-model) were assumed for entropy of fusion, S_c, and diffusion coefficient, and the liquid-solid interfacial energy, σ, was estimated with a relationship between σ and S_c due to Turnbull. These properties were then used to compute values of growth rate versus undercooling for the Flight 1 experiment and nucleant wetting angle versus undercooling for the Flight 2 experiment. From these values it was learned that the first sample did indeed undercool by an amount between 1°K and 4°K, and that superheating of the melt prior to launch of the second sample dissolved or "denucleated" all nucleants characterized by wetting angles up to 62°. Denucleation of the Flight 2 experiment had already been advanced as the reason for its failure to solidify. The theoretical analysis provided a quantitative description of the denucleation.

Flight Experiment Materials Selection

One task of this study was to select two material systems for micro-gravity experimentation for the purpose of comparison of theory and experiment. A major problem in comparing theory to experiment is the unavailability of established values for the liquid state properties of materials - especially alloys. There is virtually no data on the melt properties of multi-component materials, and very little data on melts of elements. Even though there is no good method of calculating alloy melt properties even when the elemental component property values are known, it is felt that theory-experiment comparison could best be carried out with materials systems for whose component elements the pertinent melt properties are known. In addition to the availability of melt property data, the following criteria influenced the selection of material systems for flight experimentation:

- Abundance of previously published ground-based research on the material system which may prove pertinent to Space Processing objectives.

1.3 (Continued)

- The practical (economic) importance of gaining more knowledge about the material system,
- The extent to which the material system properties improve the ability to study a particular phenomenon, and
- The general simplicity of the material system with respect to experiment design and theoretical analyses.

Based on these criteria, the material systems selected are iron-nickel and lead-tin. The melt properties for these elements are given in Table VII.

1.4 CONCLUSIONS AND RECOMMENDATIONS

The major conclusions of this study are as follows:

1. Classical heterogeneous nucleation theory is at present the simplest method for performing calculations of solidification phenomena. The validity of some assumptions in the theory have yet to be established, and its accuracy is impaired by a lack of values for the melt properties which comprise the input to the theory. But these problems also exist in the modern theories of nucleation, which are conceptually and computationally more complicated.

2. Gravitational settling (segregation) of dense phase nuclei in a melt is described by the equation

$$\left[\frac{B_1 C + B_2}{B_1 C_o + B_2}\right]^{\left(\frac{A_4}{B_1} - \frac{v'}{B_2}\right)} \left(\frac{C}{C_o}\right)^{v'/B_2} = e^{\gamma g z}$$

where C is solute concentration, g is acceleration due to gravity and z is axial position in the melt. γ is a parameter which depends on undercooling. The other factors are combinations of melt properties which are constant for a given material.

1.4 (Continued)

3. The segregation of lead and tin dendrites observed in Pb-Sn eutectic material experiments in the MSFC centrifuge, can be only partly explained by the settling theory discussed above. The linear dependence of concentration on undercooling, at fixed z, is as yet unexplained.

4. The maximum undercooling attainable in pure melts is determined by the intermolecular potentials in the liquid and solid phases of the material.

5. The amount of undercooling achieved in the December 1975 SPAR flight experiment with ammonium chloride solution was predicted by theory to be between 1°K and 4°K. Classical theory also predicts that the May 1976 SPAR ammonium chloride flight experiment was denucleated to the extent that all nucleants characterized by wetting angles of up to 62° were dissolved into the melt.

6. There is strong theoretical and experimental evidence that growth rate of a solid into its melt is a function of the undercooling squared.

7. Physical properties of solids can be related to grain size through phonon scattering theory, but mathematically, the dependence of these properties on grain size is weak compared to their dependence on temperature.

8. It should be possible to develop a solidification model which would predict grain size and dendrite morphology as a function of undercooling and nucleant characteristics. The major obstacle appears to be the lack of melt property and nucleant characteristic data for input to the model. It may also be possible to develop a comprehensive material property prediction model which would facilitate the design of materials to meet specific, predetermined requirements by calculating the material composition and solidification environment (gravity level, temperature profile, container type or absence) needed to produce the desired material.

1.4 (Continued)

9. Two material systems which are well suited to the comparison of theoretical predictions to experimental reality and to the objectives of the Space Processing program are the systems iron-nickel and lead-tin.

Based on these conclusions, it is recommended that there be further study of:

a. Computational methods and their accuracy within nucleation theories,

b. The relation of undercooling to solid structure, including the solute segregation effects observed at MSFC,

c. The relation of solid structure to all properties of the solid,

d. The relation of liquid, solid and nucleant structure to the nucleant parameters (θ, $\Delta\sigma$) and to undercooling.

Additional recommendations are:

e. That experimental measurements be made in microgravity of undercooling, nucleation rate, growth rate, grain size and morphology in the Pb-Sn and Fe-Ni systems,

f. That a program be initiated for the measurement and/or calculation of liquid state (melt) properties of engineering materials, such as the Fe-Ni alloy system,

g. That development of a comprehensive material property prediction model be undertaken. Such a model would be used as a guide for Space Processing experiment definition and design, as a guide for selection of materials for Space Processing experiments which show promise of commercial value, and as a molecular-level materials design tool.

PART 2 - DETAILS OF STUDY RESULTS

2.1 THEORIES AND MODELS OF NUCLEATION

The solidification process is possibly the least well understood phenomena of those which are common to everyday life. This is demonstrated by the plethora of theories and models which have been developed to attempt a quantitative description of the process, and by the failure of most of these models to explain any large body of experimental observation. These models as a group do, however, provide significant insight into solidification phenomena, and a specific model properly applied over a limited range can yield quantitative predictions which agree quite well with the experimental data it seeks to explain. Also, the theories and models about to be discussed are the best available mathematical tools for making predictions about nucleation. This study is concerned with solidification from the melt, so theories of nucleation of a condensed phase from vapor will not be considered explicitly, although much of the mathematical formalism is common to both nucleation events. The basic goal of most nucleation theories is to calculate a nucleation rate of the form

$$I = I_o' e^{-\frac{\Delta G_D}{kT}} e^{-\frac{\Delta G^*}{kT}} \qquad (1)$$

where

I_o' is a frequency term (nuclei/time/volume)

ΔG_D is an activation energy term for diffusion across a liquid-solid interface

ΔG^* is the free energy required for formation of a critical nucleus.

The different models are required to calculate the terms I_o', ΔG_D and ΔG^* for different physical situations.

2.1.1 Homogeneous Nucleation - Classical Theory

Classical nucleation theory has been derived from absolute rate theory by Becker and Döring [1],Becker [2],Turnbull and Fisher [3],Turnbull [4], Hollomon and Turnbull [5] among others [6]. Homogeneous nucleation refers to the spontaneous formation of solid nuclei in the melt of a pure material. A spherically shaped nucleus will be assumed to demonstrate the classical approach.

The free energy of formation for a spherical nucleus is

$$\Delta G = -\frac{4}{3}\pi r^3 \Delta G_V + 4\pi r^2 \sigma \qquad (2)$$

where $\Delta G_V = S_c \Delta T$ is the bulk free energy with S_c being the entropy of solidification and ΔT the undercooling $(T_m - T)$. σ is the surface energy at the nucleus-melt interface. Maximizing ΔG with respect to nucleus radius, r, yields the expression for the critical radius

$$r^* = \frac{2\sigma}{\Delta G_V} \qquad (3)$$

Substitution of (3) in (2) gives the critical free energy

$$\Delta G^* = \Delta G(r^*) = \frac{16\pi \sigma^3}{3 S_c^2 \Delta T^2} \qquad (4)$$

If there is reason to assume nuclei of different shape, the procedure remains the same, but models of different nuclei shape yield:

Cylinder: $r^* = \frac{2\sigma}{\Delta G_V}$, $h^* = \frac{4\sigma}{\Delta G_V}$, $\Delta G^* = 8\pi \frac{\sigma^3}{(\Delta G_V)^2}$

Parallelepiped: $a^* = \frac{4\sigma_a}{\Delta G_V}$, $b^* = \frac{4\sigma_b}{\Delta G_V}$, $c^* = \frac{4\sigma_c}{\Delta G_V}$, $\Delta G^* = 32 \frac{\sigma_a \sigma_b \sigma_c}{(\Delta G_V)^2}$.

2.1.1 (Continued)

Several attempts have been made to determine I_o and ΔG_D. Some of the more useful results are:

- Turnbull and Fisher[3]: $I_o' = n^* C \frac{kT}{h} \left(\frac{a\sigma}{9\pi kT}\right)^{1/2}$ (5a)

  where n^* is the number of atoms in the surface of a critical nucleus,

  C is the number of atoms per volume in the melt,

  h is Planck's constant,

  and a is a parameter dependent on nucleus shape.

- Free volume model[7]: $I_o' e^{-\frac{\Delta G_D}{kT}} = \frac{CD}{r_o^2}$ (5b)

  where r_o is the radius of an atom of the subject material.

In practical calculations of nucleation rate, however, I is so sensitive to $\exp(-\Delta G^*/kT)$, that the remaining terms may be approximated by a constant $I_o = I_o' \exp(-\Delta G_D/kT)$. It has also been shown [4] that for several material systems, I_o may be taken to be

$$I_o = 10^{33} = e^{75.985}$$

with very little error in the final value of I [6]. So this is the value used for I_o in this document.

2.1.2 Homogeneous Nucleation - Modern Theory

Modern homogeneous nucleation theory attempts to calculate the free energy changes associated with nucleus formation (whatever the mode of formation) from statistical mechanics. This always involves the computation of a partition function, Q, since the free energy of a material system in a condensed state is derived from the partition

2.1.2 (Continued)

function by

$$G = F = -kT \ln Q \tag{6}$$

where F is the Helmholtz free energy.

Replacement Partition Function

An important portion of modern nucleation theory deals with the calculation of a "replacement" partition function, q_{rep}.

The partition function for a nucleus containing n molecules in a melt containing C(n) nuclei per unit volume is [8]

$$Q = \left[\frac{1}{C(n)!}\right]^{\frac{1}{C(n)}} \frac{\lambda q_r}{q_{rep}} \exp\left[-\frac{\sigma A(n)}{kT} - \frac{n\mu}{kT}\right] \tag{7}$$

where $\lambda = h^{-3}(2\pi nmkT)^{3/2}$ is the translational partition function,

$q_r = h^{-3}(2kTI)^{3/2}\sqrt{\pi}$ is the rotational partition function, I being the moment of inertia, $\frac{2}{3}nmr^2$, of the nucleus, σ is the liquid-solid interfacial energy, A(n) is the surface area of the nucleus, and μ is the chemical potential of the bulk solid.

The replacement partition function arises from the following consideration. When a nucleus forms from a melt, the atoms in the nucleus give up degrees of freedom which are replaced by six translational and rotational degrees of freedom for the nucleus as an entity in the melt, with the relative positions of the atoms in the nucleus remaining fixed. That is, q_{rep} yields correction terms for the thermodynamic functions which are necessary to extend the validity of these macroscopic functions to non-macroscopic systems such as nuclei. Hence the name "replacement" partition function. Another way to view this process is that as the atoms arrange themselves in the ordered structure of the nucleus, the

2.1.2 (Continued)

entropy of the system is lowered, giving rise to an increase in free energy, calculated from

$$G_{rep} \approx kT \ln q_{rep} \quad . \tag{8}$$

Crystal Subdivision

One approach followed in modern nucleation theory is to calculate the change in free energy of a nucleus due to a change in surface area from partition functions for the system before and after the change. Part of this approach considers extension of a crystal surface, while another part considers the energy change when a crystal is subdivided. In the latter part, the free energy per crystallite (which divided itself from the parent crystal of n atoms) is

$$\Delta G_2 = e_x^o A_x - kT \ln(q_t\, q_r) - kT + \sum_{j=1}^{3x-6} (\phi_j + n_j) - \frac{1}{m} \sum_{i=1}^{3n-6} (f_i + \varepsilon_i) \tag{9}$$

where there are m nuclei containing x molecules for a total of n = mx molecules in the solid, and where

$e_x^o A_x$ = increase in potential energy of a nucleus with surface area A_x,

q_t, q_r = translational and rotational partition functions,

f_i, ϕ_j = free energies of the i^{th} and j^{th} oscillation modes,

ε_i, n_j = zero point free energies of the i^{th} and j^{th} modes.

The i subscripts refer to the bulk, undivided crystal, while the j subscripts refer to internal vibrations of each crystallite. In terms of the classical surface free energy, $\sigma_\infty = e_\infty - Ts_\infty$, this is:

2.1.2 (Continued)

$$\Delta G_2 = \sigma_\infty A_x - kT\, \ell n(q_t\, q_r) - kT + kT\, \ell n\, K'_x \qquad (10)$$

where

$$kT\, \ell n\, K'_x = (e^o_x - \sigma_\infty)A_x + \sum_{j=1}^{3x-6} (\phi_j + \eta_j) - \frac{1}{m} \sum_{i=1}^{3n-6} (f_i + \epsilon_i) \quad . \qquad (11)$$

Evaluation of $kT\, \ell n\, K'_x$ is a central problem in modern nucleation theory. This has not yet been done rigorously, but some prescriptions have been given for approximate evaluation. [9]

- Frenkel Prescription: $kT\, \ell n\, K'_x = -\frac{4\sigma_\infty}{3x} - 2\sigma_\infty$

  Note: the subscript ∞ refers to a flat surface.

- Kuhrt Prescription: $kT\, \ell n\, K'_x = -2\mu_{II\infty}$

  Note: $\mu_{II\infty}$ = crystal chemical potential.

- Lothe-Pound Prescription: $kT\, \ell n\, K'_x = (\sigma_x - \sigma_\infty)\, A_x + 2\, \frac{Ts_\infty}{N_o}$

2.1.3 Heterogeneous Nucleation Theory and Models

Heterogeneous nucleation refers to the formation of a nucleus of some shape on a foreign substrate, whether this substrate is a container surface, the surface of a contaminant particle or the surface of a particle of a high temperature phase of the melt material itself. Equation (1) holds for heterogeneous nucleation as well as for homogeneous nucleation if the appropriate expressions for I_o, ΔG_D and ΔG^* are used. Equation (2) is generalized as follows

$$\Delta G = -n(\mu_\ell - \mu_s) + \sigma\, A \qquad (12)$$

where n = number of moles in a nucleus

μ_ℓ, μ_s = chemical potential of liquid and solid respectively

σ = interfacial energy

A = area of liquid-solid interface (any shape).

2.1.3 (Continued)

The difference in potential, $\mu_\ell - \mu_s$, is called the driving force for solidification, and the volume potential is defined by

$$\Delta\mu_v = \frac{\mu_\ell - \mu_s}{v} = \Delta G_v = S_c \, \Delta T \qquad (13)$$

where v is molar volume. The derivation of the classical example of a spherical cap nucleus will be given, then the results of critical parameters for other geometries will be quoted.

Spherical Cap Nucleus

Figure 1 shows a schematic of a spherical cap nucleus, n, on some kind of substrate, s. The cap's radius is r, and the interfacial energies between liquid and substrate, ℓs, liquid and nucleus, $n\ell$, and nucleus and substrate, sn, are as shown. (Actually, interfacial energy, σ, is a scalar quantity, and the vectors shown are of interfacial tensions, which are vector quantities; but in most cases the magnitude of an interfacial tension is numerically equal to the interfacial energy, particularly if there is little or no temperature dependence of these quantities).

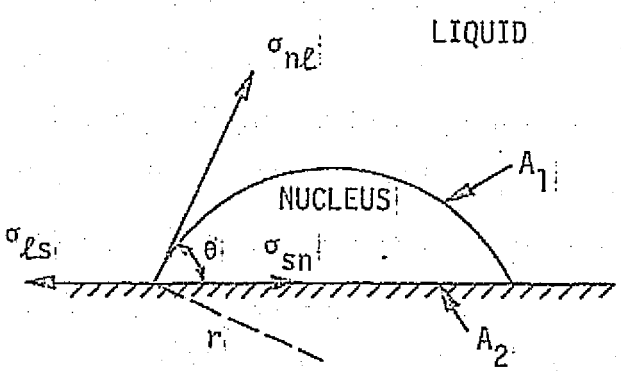

FIGURE 1 SPHERICAL CAP NUCLEUS

In this case, equation (12) becomes

$$\Delta G^* = - nV \, \Delta\mu_v + \sigma_{n\ell} A_1 + (\sigma_{sn} - \sigma_{s\ell}) \, A_2 \qquad (14)$$

2.1.3 (Continued)

If R is the radius of the cap nucleus-substrate interface, then from Figure 1

$$A_2 = \pi R^2 = \pi r^2 \sin^2\theta = \pi r^2 (1-\cos^2\theta)$$

since $R = r \cos(\frac{\pi}{2} - \theta) = r \sin\theta$. Standard mensuration formulae may be used to find the surface area and volume of the nucleus

$$A_1 = 2\pi r (r - r\cos\theta) = 2\pi r^2(1-\cos\theta)$$

$$V = \frac{1}{3}\pi (r - r\cos\theta)^2 [3r-(r-r\cos\theta)] = \frac{\pi}{3} r^3 (2+\cos\theta)(1-\cos\theta)^2$$

or

$$V = \frac{4}{3}\pi r^3 f(\theta)$$

where $f(\theta) = \frac{1}{4}(2 + \cos\theta)(1 - \cos\theta)^2$. Thus equation (14) becomes

$$\Delta G = -\frac{4}{3}\pi r^3 f(\theta) n \Delta\mu_V + 2\pi r^2(1-\cos\theta)\sigma_{n\ell} + \pi r^2(1-\cos^2\theta)(\sigma_{Sn}-\sigma_{S\ell}) . \quad (15)$$

This equation can be simplified by noting from Figure 1 that

$$\sigma_{sn} - \sigma_{\ell s} = -\sigma_{n\ell}\cos\theta . \quad (16)$$

Thus, after performing the algebraic manipulation, one obtains

$$\Delta G = -\frac{4}{3}\pi r^3 f(\theta) n\Delta\mu_V + 4\pi r^2 \sigma_{n\ell} f(\theta). \quad (17)$$

Maximizing ΔG with respect to r in the standard fashion

$$\frac{\partial \Delta G}{\partial r}\Big|_{r^*} = 4\pi f(\theta)[2\sigma_{n\ell} r^* - r^{*2} n\Delta\mu_V] = 0. \quad (18)$$

2.1.3 (Continued)

Thus the critical (sphere) radius per mole of the nucleus is

$$r^* = \frac{2\sigma_{n\ell}}{\Delta\mu_V} = \frac{2\sigma_{n\ell}}{S_c \Delta T} \tag{19}$$

which is the same as for the homogeneous case. Substituting (19) in (17), one obtains for the critical free energy

$$\Delta G^* = \frac{16\pi\ \sigma_{n\ell}^3}{3\Delta\mu_V^2}\ f(\theta) \tag{20}$$

which differs from the homogeneous case only by the "heterogeneous nucleation function," $f(\theta)$ where θ is called the "wetting angle".

Models of Other Nucleus Geometries

To discuss other geometries it is convenient to define the "heterogeneous nucleation parameter," $\Delta\sigma$, by

$$2\Delta\sigma = \sigma_{n\ell} - \sigma_{\ell s} + \sigma_{sn} \quad . \tag{21a}$$

Related to the spherical cap model, this is just

$$2\Delta\sigma = \sigma_{n\ell}\ (1 - \cos\theta). \tag{21b}$$

However, in other nucleus geometries where θ has no meaning, the critical parameters may be written in terms of the heterogeneous nucleation parameter as is done in these two examples [10].

Cylinder: $r^* = \frac{2\sigma_{n\ell}}{\Delta\mu_V}$, $h^* = \frac{4\Delta\sigma}{\Delta\mu_V}$, $\Delta G^* = 8\pi \frac{\sigma_{n\ell}^2 \Delta\sigma}{(\Delta\mu_V)^2}$

Parallelepiped: $a^* = \frac{4\Delta\sigma}{\Delta\mu_V}$, $b^* \frac{4\sigma_b}{\Delta\mu_V}$, $c^* = \frac{4\sigma_c}{\Delta\mu_V}$, $\Delta G^* = 32 \frac{\sigma_b \sigma_c \Delta\sigma}{(\Delta\mu_V)^2}$.

2.1.3 (Continued)

Kossel Crystal

One of the simplest heterogeneous nucleation models is the Kossel crystal, shown in Figure 2. The basic assumption in this model is that the energy of attachment of a molecule to the nucleus is given in terms of the nearest-neighbor interaction energy, ϕ. It is also assumed that, since the nucleus is orthorhombic and the molecules fit into a rectangular lattice, the interaction energy is related to the interfacial free energies by

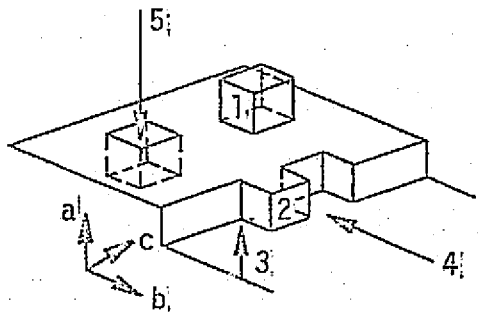

FIGURE 2 KOSSEL CRYSTAL

$$\phi_a = 2b_o c_o \sigma_a ; \quad \phi_b = 2a_o c_o \sigma_b ; \quad \phi_c = 2a_o b_o \sigma_c$$

where the "a"face is that face orthogonal to the "a" direction in the crystal and bounded by sides b and c. The a_o, b_o and c_o are the dimensions of a single molecule in the lattice. Since the free energy of formation of a nucleus is in general

$$\Delta G = \sum_i \sigma_i A_i - \Delta\mu_v V \quad , \tag{22}$$

for the rectangular nucleus we have

$$\Delta G = 2bc\sigma_a + 2ac\sigma_b + 2ab\sigma_c - abc\,\Delta\,\mu_v \quad . \tag{23}$$

The critical values of the nucleus dimensions and the free energy are found by maximizing ΔG with respect to a, b and c, and are

$$a^* = \frac{4\sigma_a}{\Delta\mu_v} \; , \; b^* = \frac{4\sigma_b}{\Delta\mu_v} \; , \; c^* = \frac{4\sigma_c}{\Delta\mu_v} \tag{24}$$

and

$$\Delta G^* = 32\,\frac{\sigma_a\sigma_b\sigma_c}{(\Delta\mu_v)^2} \tag{25}$$

2.1.3 (Continued)

Nucleus-Substrate Lattice Disregistry

In earlier work [11] on undercooling of multiphase alloy systems, it was suggested that tiny particles of high temperature phases extant in the melt could act as heterogeneous nucleation sites for the lower temperature phases and prevent their undercooling. The theoretical approach to the problem of determining whether particles of a high temperature phase act as "nucleation catalysts" would be to ask first whether high temperature phase particles are more effective as heterogeneous nucleants than other impurities in the melt. If the answer to this question is yes, high temperature phase particles are more effective nucleants, the next question is, why?

The original work (pertinent to this question) by Turnbull and Vonnegut [12] defined a disregistry parameter, δ by

$$\delta = \frac{\Delta a}{a_o} \tag{26}$$

where a_o is the dimension of the unit cell of the solid material being nucleated and Δa is the amount by which the dimension of the nucleant (substrate) unit cell exceeds a_o. Turnbull and Vonnegut concluded from the data available at that time that the smaller the disregistry, δ, the more effective as a nucleant was the particle or substrate catalyzing nucleation. They even showed that the free energy of solidification required to produce a perceptible nucleation rate was proportional to δ^2. However, subsequent experimental work by Sundquist and Mondolfo [13], essentially disproves Turnbull and Vonnegut's theory showing that: (a) substrates or impurities with high disregistries are as good nucleating agents as substrates with low disregistries, (b) symmetry of the lattice plane orientation (across the mating plane) is at least as important as disregistry in catalyzing nucleation, and (c) neither the orientation relationship nor the disregistry appear to have any effect on the undercooling (and hence driving force, i.e., Gibbs free energy) required for nucleation. Yet work by Glicksman and Childs [14] at almost the same time

2.1.3 (Continued)

found a qualitative relation between disregistry and undercooling, more or less in agreement with Turnbull and Vonnegut. Hence the question of the influence of substrate (or impurity) surface structure on the value of undercooling at which nucleation occurs remains unanswered, and it must be answered before progress can be expected on determining the influence of high temperature phase particles on the melt. In fact, experimental studies of certain alloy systems show that neither oxides nor carbides were as effective as nucleants for lower temperature phases as might be expected, nor were they as effective as particles of unknown contaminants present in the melts of the lower temperature phases [6]. This would indicate that concern over the effectiveness of high temperature phase particles as nucleants is no more justified than for any other contaminant in the melt. But there is no doubt that the lattice structures at the nucleus-substrate interface are important for determining the effectiveness of the substrate as a nucleation catalyst, even if the structure effect should manifest itself only in the interfacial energies shown in Figure 1. This is one area of Materials Science where a major research effort is urgently needed. It is possible that the theoretical portion of this research should proceed along the lines to be suggested in Section 2.2.1.

2.1.4 Nucleation in Two Component Melts

Nucleation in two-component melts can best be understood with the help of the free energy-composition diagram shown in Figure 3. The parameters to be calculated are the critical radius of the nucleus, r*, and the critical free energy for nucleus stability, ΔG^*. The change in bulk free energy upon formation of a nucleus can be expressed as the sum of the free energies after formation minus the melt free energy before formation [15]

ΔG_m = % of atoms in nucleus X G of solid

+ % of atoms in depleted melt X G of depleted melt

- G of original melt

2.1.4 (Continued)

or, as can be seen from Figure 3, for a nucleus of composition X_2 which solidifies from an original melt of composition X leaving a depleted melt of composition X_1,

$$\Delta G_m = \frac{N_2}{N} G_{X_2} + \frac{N_1}{N} G_{X_1} - G_X \quad . \tag{27}$$

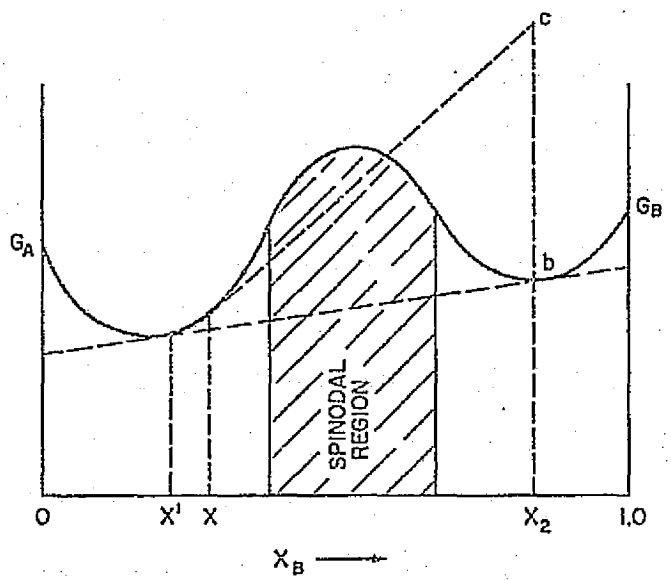

FIGURE 3 GIBBS FREE ENERGY OF A TWO-COMPONENT MATERIAL

Here $N_1 + N_2 = N$ where N_2 is the number of atoms in the nucleus, N_1 is the number of atoms in the depleted melt and N is the total number of atoms in the binary system. Thus (27) can be rewritten

$$\Delta G_m = \frac{N_2}{N} (G_{X_2} - G_X) + \frac{N_1}{N} (G_{X_1} - G_X) \quad . \tag{28}$$

The following compositional relationship holds:

nucleus atoms [nucleus composition - pure melt composition] =

depleted melt atoms [pure melt composition - depleted melt composition]

2.1.4 (Continued)

or

$$N_2 (X_2 - X) = N_1 (X - X_1)$$

which is

$$\frac{N_1}{N_2} = \frac{X - X_2}{X_1 - X} \quad . \tag{29}$$

Substituting (29) in (28), by noting that $\frac{N_1}{N} = \frac{N_2}{N} \cdot \frac{N_1}{N_2}$, yields

$$\Delta G_m = \frac{N_2}{N} \left[G_{X_2} - G_X + \frac{X - X_2}{X_1 - X} (G_{X_1} - G_X)\right] \quad . \tag{30}$$

Expressing $\frac{G_{X_1} - G_X}{X_1 - X}$ as a differential instead of a difference, (30) becomes

$$\Delta G_m = \frac{N_2}{N} \left[G_X - G_{X_2} + (X_2 - X) \left(\frac{dG}{dX}\right)_X\right] \quad . \tag{31}$$

The total free energy change on nucleus formation is the sum of volume and surface terms

$$\Delta G = -\frac{4}{3} \pi r^3 \left[\frac{\Delta G_m}{N\{X_2 v_B + (1-X_2) v_A\}}\right] + 4\pi r^2 \sigma \tag{32}$$

where σ is the liquid-solid interfacial energy for the binary alloy, r is the radius of the nucleus, and v_B and v_A are the specific volumes of components B and A respectively. Thus the denominator of the first term is simply the total system volume. Maximizing ΔG with respect to r leads directly to the critical radius

$$r^* = \frac{2\sigma N[X_2 v_B + (1-X_2) v_A]}{\Delta G_m} \tag{33}$$

2.1.4 (Continued)

and hence to the critical free energy

$$\Delta G^* = \frac{16\pi\sigma^3 N^2 [X_2 v_B + (1-X_2)v_A]^2}{3\ \Delta G_m^{\ 2}} \qquad (34)$$

From equation (34), the nucleation rate in the alloy can now be calculated from the usual relation

$$I = I_o \exp\left[- \frac{\Delta G^*}{kT} \right]$$

2.2 THEORETICAL TECHNIQUES RELATING TO UNDERCOOLING, EFFECTS OF GRAVITY ON MELTS AND SOLIDIFICATION

2.2.1 The Relation of Undercooling to Intermolecular Potentials

The undercooling of liquids is of considerable importance in industrial solidification processes [16,17], in the study of the liquid-solid transition [18-24], and as an interesting phenomena in its own right [25-28]. One fundamental question to be answered about the undercooling of pure liquids can be stated: "Why does one liquid material undercool more (or less) than another?" For simplicity, the following discussion of this question will be limited to impurity-free, single-component liquids.

The most extensive experimental work applicable to the above question is the study of maximum undercooling and homogeneous nucleation performed twenty-five years ago by Turnbull [23,24], and his data are still the most widely quoted in the literature. The important result of Turnbull's experiments, which used the "small drop" technique to ensure purity and homogeneous nucleation, was the establishment of a reproducible maximum value of undercooling, ΔT_{max}, at which each liquid material nucleates homogeneously. The question of why these materials nucleate homogeneously at a characteristic undercooling has been largely ignored, except for discussions of the relation of undercooling and solidification to liquid structure [4,25]. To state that the amount of undercooling a pure material melt will sustain depends on the structure of the solid to which it solidifies is almost equivalent to stating that the undercooling depends on the intermolecular potentials in the solid phase of the material. It is the purpose of this report to show that, within the framework of classical homogeneous nucleation theory, the maximum undercooling obtainable before a given material solidifies can be related (at least formally) to the intermolecular potentials in both the liquid and solid phases.

RELATION OF UNDERCOOLING TO MACROSCOPIC PROPERTIES

The classical homogeneous nucleation rate, I $(\frac{\text{nuclei}}{\text{cm}^3\text{sec}})$, is given by [20]

$$I = I_o e^{-\left(\frac{A}{\Delta T}\right)^2} \tag{35}$$

where, for spherical nuclei,

$$A^2 = \frac{16\pi\ \sigma^3}{3kT\ S_c^{\ 2}}$$

or

$$A = 4\sqrt{\frac{\pi}{3kT}}\ \frac{\sigma^{3/2}}{S_c} \tag{36}$$

where T is absolute temperature, σ is the liquid-solid interfacial energy, S_c is the entropy of fusion and k is Boltzmann's constant. According to Turnbull [4],

$$I_o \approx 10^{33} \approx e^{76}\ \ \frac{\text{nuclei}}{\text{cm}^3\text{sec}}$$

thus

$$I = \exp\left[76 - \left(\frac{A}{\Delta T}\right)^2\right] \tag{37}$$

Obviously, the largest undercooling a liquid can sustain is the largest value of ΔT which leaves I in equation (37) essentially zero. If one takes this value of I to be less than or equal to some small, constant value, ξ, then from equation (37)

$$76 - \left(\frac{A}{\Delta T}\right)^2 \leq \ell n\ \xi$$

2.2.1 (Continued)

or

$$\Delta T \leq \frac{A}{\sqrt{76 - \ell n\, \xi}} \quad . \tag{38}$$

Therefore, the larger the value of A, or by equation (36) the larger the value of $\frac{\sigma^{3/2}}{S_c}$, for a given material, the larger undercooling, ΔT_{max}, the material will sustain. A rigorous test of how well this classical prediction agrees with experiment must await further application of a direct technique for measuring interfacial energies, such as that developed by Glicksman and Vold [29]. This is because most published values of σ were calculated from nucleation data via equation (37) [19], since the Glicksman and Vold technique has not been applied to many liquids. It is no surprise, then, that values of A calculated for various liquids using Turnbull's values for σ [23] should correlate with measured ΔT_m values as well as they do in Figure 4. Data for calculating A values are given in Table I. Note that I and ΔT_{max} are the variables measured by Turnbull, and that S_c $(=\frac{Q}{T_m})$ is the other "known" parameter used to calculate σ from the nucleation experiments.

RELATION OF S_c TO INTERMOLECULAR POTENTIALS

Since entropy is a state function, the entropy of fusion is calculated from the partition function by [30]

$$S_c = k\, \ell n \frac{Z_L}{Z_S} + kT \left[\frac{\partial}{\partial T} \left(\ell n \frac{Z_L}{Z_S}\right)\right]_V \tag{39}$$

where Z_L is the liquid partition function and Z_S is the solid partition function. In the canonical ensemble, the partition function is given by the rigorous relation [30]

$$Z_{L,S}\,(V,T) = \int \frac{d^{3N}p\, d^{3N}r}{N!\, h^{3N}}\, e^{-\frac{H_{L,S}\,(p,r)}{kT}} \tag{40}$$

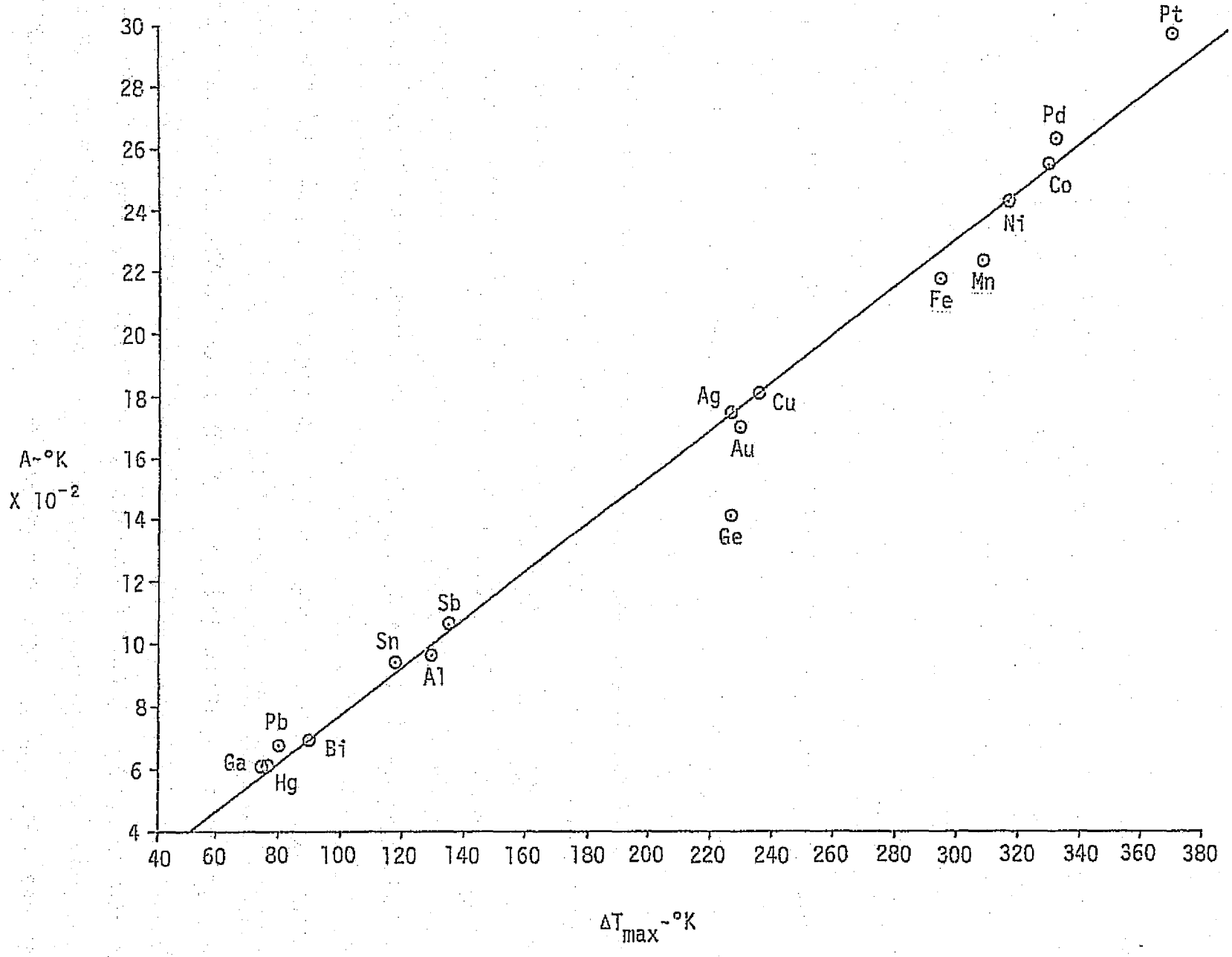

FIGURE 4 A VS. ΔT FROM TURNBULL'S DATA

TABLE I DATA FOR CALCULATING VALUES OF A (from Turnbull [23])

MATERIAL	σ erg/cm^2	Q $10^9 \frac{erg}{cm^3}$	T_M °K	S_c $10^6 \frac{erg}{cm^3 °K}$	ΔT_{max} °K	T °K	A °K
Mercury	28.1	1.583	234.6	6.747	77	157.6	612.7
Gallium	56.0	4.752	302.8	15.693	76	226.8	617.8
Tin	59.0	4.415	504.9	8.528	118	386.9	941.3
Bismuth	54.4	5.107	544.0	9.388	90	454.0	698.8
Lead	33.3	2.789	600.0	4.340	80	520.0	676.5
Antimony	101.0	10.778	903.0	11.936	135	768.0	1069.0
Aluminum	93.0	10.669	931.7	11.451	130	801.7	963.7
Germanium	181.0	23.38	1231.7	18.982	227	1004.7	1410.0
Silver	126.0	10.97	1233.7	8.892	227	1006.7	1746.6
Gold	132.0	12.429	1336.0	9.303	230	1106.0	1707.0
Copper	177.0	18.327	1356.0	13.515	236	1120.0	1813.9
Manganese	206.0	19.816	1493.0	13.273	308	1185.0	2254.5
Nickel	255.0	26.689	1725.0	15.472	318	1407.0	2444.5
Cobalt	234.0	22.731	1763.0	12.893	330	1433.0	2555.0
Iron	204.0	21.627	1803.0	11.995	295	1508.0	2179.3
Palladium	209.0	18.804	1828.0	10.287	332	1496.0	2645.7
Platinum	240.0	21.61	2042.0	10.583	370	1672.0	2993.4

2.2.1 (Continued)

where N is the number of molecules in the solidifying system, h is Planck's constant, p represents molecule momenta, r represents molecular position and $H_{L,S}(p,r)$ is the Hamiltonian for the system of molecules in the liquid or solid state, respectively.

In the liquid state, the Hamiltonian is usually written as [31]

$$H_L = \sum_i \frac{p_i^2}{2m} + \sum_{i>j} \phi_L(r_{ij}) \tag{41}$$

where $\phi(r_{ij})$ is the potential energy between molecules i and j in the liquid. The intergration over momenta may be performed in a straightforward manner to yield

$$Z_L = \frac{\lambda^{-3N}}{N!} \int_V \exp\left[-\frac{\sum_{i>j} \phi_L(r_{ij})}{kT}\right] d^{3N}r \tag{42}$$

where λ is the "thermal wavelength"

$$\lambda = \sqrt{\frac{h^2}{2\pi m\, kT}} \quad .$$

The evaluation of the "configuration integral" in equation (42) is the central problem of liquid state physics and only approximate solutions based on a variety of simplifying assumptions have been obtained to date [32]. However, equations (39) and (42) do show explicitly the dependence of S_c on liquid intermolecular potentials.

A choice of models is also available for evaluation of the partition function in the solid state. Perhaps the Einstein model of a solid is the simplest model to have been reasonably successful in predicting solid properties [33]. In this model, the partition function is

$$Z_S = \prod_{i=1}^{3N} \left(1-e^{-\frac{\hbar\omega_i}{kT}}\right)^{-1} \tag{43}$$

2.2.1 (Continued)

where the ω_l are the phonon frequencies derived from the Hamiltonian for the solid lattice of N molecules which is approximated by a sum of terms, each representing a harmonic oscillator. The frequences in the harmonic oscillator approximation are related to the intermolecular potentials by

$$\phi_S(r_{ij}) = \frac{1}{2} m \omega_i^2 r_{ij}^2 \quad . \tag{44}$$

This completes the formal relationship between entropy of fusion and intermolecular potentials in the solid and liquid states.

RELATIONSHIP OF σ TO INTERMOLECULAR POTENTIALS

Although the liquid-solid interfacial energy, σ, is of major importance to most nucleation and solidification models*, it has remained one of the most difficult parameters to measure directly by experiment or to calculate theoretically. The reasons for the theoretical difficulties arise primarily from the inability to describe liquid structure, particularly in the interface region. Some recent work by Spaepen [34] based on the random packing of hard spheres model developed by Bernal and coworkers [35-37], derives an expression for σ in terms of the

*In common practice, little distinction is made between the interfacial energy, σ, and the interfacial tension, $\vec{\gamma}_i$. The primary distinction between the two is that σ is a scalar energy per unit area while $\vec{\gamma}$ is a vector force per unit length. There is also the thermodynamic relationship

$$\sigma = \gamma_i - T \left(\frac{\partial \gamma_i}{\partial T}\right)_{V,A}$$

where γ_i is the magnitude of $\vec{\gamma}_i$, which further differentiates between σ and γ_i.

2.2.1 (Continued)

configurational entropies of the interface and the bulk material. This treatment is strictly structural, and the interface whose properties are studied is itself built according to the construction rules which apply in the random packed phase. This approach therefore shows no explicit relation between σ and the intermolecular potentials, but certainly these potentials must play some role in establishing the random packed structure from which the construction rules are derived.

The most obvious formal relationship of σ to intermolecular potentials is found in the thermodynamic expression for σ as the change in free energy F, with interface area

$$\sigma = \left(\frac{\partial F}{\partial A}\right)_{P,T,N} .$$

F is related to the partition function for the system by

$$F = -kT \ell n Z$$

and hence to the potentials ϕ as discussed above. The difficulty occurs in deriving F(A) for a system containing a liquid-solid interface. Thus alternate approaches to the derivation of the liquid-solid interfacial energy have been pursued historically.

The theory which shows the most direct relationship between liquid-solid interfacial energy and intermolecular potentials is that due to Skapski [38]. In this theory the difference between intermolecular potentials in the solid and liquid phases appears explicitly in the equation for σ. In actual computations, the difference in intermolecular potentials is replaced by a function of the heat of fusion. Skapski's theory, although simple, yields values of σ which are in order-of-magnitude agreement with those obtained by Turnbull from nucleation experiments (see Table I). However, both this theory and that developed by Turnbull [39], which is similar to Skapski's theory in the dependence of σ on intermolecular potentials, are based on a general randomness of the liquid (and perfect crystallinity of the solid), and use no specific structural information.

2.2.1 (Continued)

A rigorous analysis of liquid-solid interfacial energy given by Herring [40] was used by Glicksman and Vold [29] as a basis for their method of experimentally determining σ. This method is of particular importance since it is at present the only source of experimental values of σ which are not obtained from nucleation experiments. The theory, as applied by Glicksman and Vold, considers a symmetrical low-angle tilt boundary intersecting the liquid-solid interface under isothermal, stress-free conditions. In this case, the tilt boundary must terminate at a symmetrical groove on the liquid-solid interface. If ψ is the dihedral angle subtended by the liquid phase at the root of the groove, Glicksman and Vold show that ψ is related to the tilt angle, θ, and the liquid-solid interfacial energy by

$$\frac{1}{\theta} \cos \frac{\psi}{2} = A' - \frac{E_o}{2\sigma} \ell n\, \theta \qquad (45)$$

where A' is a constant. When the angles ψ and θ are measured experimentally, the parameter $\frac{1}{\theta} \cos \frac{\psi}{2}$ may be plotted as a linear function of $\ell n\, \theta$ with a slope

$$m = - \frac{E_o}{2\sigma} \quad .$$

Thus

$$\sigma = - \frac{E_o}{2m} \qquad (46)$$

where m is determined empirically. E_o is a factor of the Read-Shockley formulation for the internal energy per unit area of a symmetric low-angle tilt boundary, and is given by

$$E_o = \frac{G\, a}{4\pi(1-\nu)} \quad (\cos \varepsilon + \sin \varepsilon) \qquad (47)$$

where ε is the orientation angle for the boundary in a selected coordinate system, a is the lattice constant, ν is Poisson's ratio and G is the

2.2.1 (Continued)

modulus of rigidity. It should be noted here that in their theory of crystal-melt interfacial energy, Kotzé and Kuhlmann-Wilsdorf [41] derive the relation

$$\sigma = 0.85\ \theta_m \frac{Gb}{16\pi} \left[\frac{1}{1-\nu} + 2\right] \tag{48}$$

where b is the Burger's vector and θ_m is a constant angle, approximately 25°. The derivation of this equation considers the liquid-solid interface to be half of a general dislocation grain boundary, a central idea in the Kuhlmann-Wilsdorf theory of melting [42].

The importance of equation 48 and of equations 46 and 47 together is the direct dependance of σ on the modulus of rigidity in the solid, G. In most real materials, anisotropy cannot be neglected. Therefore, G will depend on the elastic constants of the material. In the Kuhlmann-Wilsdorf model the relationship is

$$G = 3\ C_{44}\ \frac{C_{11} - C_{12}}{4\ C_{44} + C_{11} - C_{12}} \tag{49}$$

while the relationship developed by Read and Shockley [43] whose theory is used by Glicksman and Vold is

$$\frac{G}{1-\nu} = (C_{11} + C_{12}) \left[\frac{C_{44}}{C_{11}}\left(\frac{C_{11} - C_{12}}{C_{11}+C_{12}+2C_{44}}\right)\right]^{1/2} \tag{50}$$

2.2.1 (Continued)

The elastic constants, C_{mn}, are the traditional form, obtained by direct contraction, of the tensor elastic constants, $C_{\alpha\beta,\gamma\lambda}$. It is the $C_{\alpha\beta,\gamma\lambda}$ which are directly related to the intermolecular potentials, being complicated linear combinations of second derivations of the configurational energy function

$$\Phi = \frac{1}{2} \sum_{i=j\pm 1} \phi(|x_i - x_j|) \tag{51}$$

in which $\phi(|x_i - x_j|)$ is the two-body potential between molecules at position x_i and at position x_j. According to Huntington [44], the dependence of $C_{\alpha\beta,\gamma\lambda}$ on Φ takes the form

$$C_{\alpha\gamma,\beta\lambda} + C_{\alpha\lambda,\beta\gamma} = 2[\alpha\beta,\gamma\lambda] + (\alpha\gamma,\beta\lambda) + (\alpha\lambda,\beta\gamma) \tag{52}$$

where

$$[\alpha\beta,\gamma\lambda] = -\frac{1}{2v_a} \sum_{l'k'k'} \frac{\partial^2\Phi}{\partial x_\alpha \partial x_\beta} \{^{\ell\ell'}_{kk'}\} x_\gamma \{^{\ell\ell'}_{kk'}\} x_\lambda \{^{\ell\ell'}_{kk'}\} \tag{53}$$

and

$$(\alpha\gamma,\beta\lambda) = -\frac{1}{v} \sum_{kk'} \sum_{\mu\nu} I_{\mu\nu}(kk') \left[\sum_{\ell''k''} \frac{\partial^2\Phi}{\partial x_\mu \partial x_\alpha} \{^{\ell\ell''}_{kk''}\} x_\gamma \{^{\ell\ell''}_{kk''}\} \right] \left[\sum_{\ell'''k'''} \frac{\partial^2\Phi}{\partial x_\nu \partial x_\beta} \{^{\ell'\ell'''}_{k'k'''}\} x_\lambda \{^{\ell'\ell'''}_{k'k'''}\} \right] . \tag{54}$$

Here v_a represents the volume per unit cell and the x_α are the components of the relative position vector between the lattice positions associated with the indices given in the curly brackets. $I_{\mu\nu}(k\ k')$ is the square matrix which is inverse to the matrix

$$\sum_{\ell} \frac{\partial^2\Phi}{\partial x_\mu \partial x_\nu} \{^{\ell\ \ell'}_{k\ k'}\} .$$

2.2.1 (Continued)

Thus the interfacial energy is seen to ultimately depend on the second derivative of the intermolecular potentials in the solid phase. Knowledge of what influence the liquid phase potentials may have on the interface structure and interfacial energy was precluded by the formulation of the Herring theory in terms of an equilibrium between the solid and liquid which leads to zero difference in free energy across the interface. In the Kuhlmann-Wilsdorf theory, the liquid is viewed as a solid with a high concentration of dislocation cores, with the interface assumed to be a modified dislocation boundary, hence the obvious dependence on solid properties. What is needed for an understanding of the fundamental origins of liquid-solid interfacial energy is a theory which combines the liquid structural considerations of Spaepen with the solid potential energy relationships demonstrated above.

SUMMARY

It has been shown, within the framework of classical physics (with the possible exception of the Einstein model), that the amount of undercooling the liquid phase of a pure material can sustain is a function of the intermolecular potentials of the material. That this conclusion may also be valid for heterogeneous nucleation on impurities or substrates is indicated by the postulated dependence of undercooling on the disregistry [12,16,45]. It might be noted that Burton [46] and others [8] have applied statistical mechanical considerations similar to those above to the general problem of nucleation from the vapor, but have not addressed the liquid-solid transition. The present work illustrates the difficulty in carrying out rigorous calculations of the characteristic maximum undercooling to be expected in real liquid systems based only on knowledge of intermolecular potentials, without making simplifying assumptions similar to those of Skapski in his nearest-neighbors model of the liquid-solid interface.

2.2.1 (Continued)

Although more realistic nucleation models than classical homogeneous nucleation theory could be used in determining characteristic maximum undercooling, predictions must eventually depend on thermodynamic values like σ and S_c. Until these quantities can be rigorously evaluated from intermolecular potentials for various materials, the formal relationships presented here must suffice as the explanation for why different pure liquids undercool different amounts.

2.2.2 Undercooling and Growth Rate

That the growth rate of dendrites and other solid interfaces into undercooled melts is proportional to the square of the undercooling is well established experimentally [47]. Theoretically, there are several ways to show the relationship. An early method, due to Chalmers [48], addresses the problem of lamellar growth of solid into the melt. By deriving relationship between geometric, kinetic and energetic properties of the lamellae, Chalmers was able to show that

$$\lambda^2 U_c = K_1 \tag{55}$$

where U_c is growth rate, K_1 is a constant and λ is the lamellar wavelength ($\frac{\lambda}{4}$ = one lamellar width), which is related to the undercooling by [48]

$$\lambda = \frac{\sqrt{K_2}}{\Delta T} \quad . \tag{56}$$

Thus

$$U_c = \frac{K_1}{K_2} \Delta T^2 \tag{57}$$

with

$$\frac{K_1}{K_2} = \frac{8 D S_c}{M_\alpha (1-k_\alpha) C_E \sigma_{\alpha\beta}} \tag{58}$$

2.2.2 (Continued)

where D = diffusion coefficient
S_c = entropy of fusion
m_α = liquidus slope
k_α = distribution coefficient
C_E = equilibrium concentration of the melt
$\sigma_{\alpha\beta}$ = interfacial energy at the α-β lamella phase boundary.

The more general solidification rate theory of Turnbull, Hillig [22] and Cohen [49] derives the expression

$$U_c = \frac{\Delta T}{A_1} [1-e^{-A_2 \Delta T}] \quad . \tag{59}$$

Expansion of the exponential and multiplication yields

$$U_c = \frac{A_2}{A_1} \Delta T^2 \tag{60}$$

plus higher order terms, with

$$\frac{A_2}{A_1} = \frac{v\ D\ S_c^2}{4\pi\ kT\ \sigma} \tag{61}$$

where v = specific volume
k = Boltzmann's constant
σ = liquid-solid interfacial energy

and other terms are as defined above. These simple relationships between growth rate and undercooling are complicated by the lack of good data for the parameters which make up K_1/K_2 and A_2/A_1, but are nevertheless most useful in the analysis and guidance of solidification experiments, as will be demonstrated in Section 2.3.

2.2.3 Interface Stability and Dendrite Formation

The way undercooling influences solid structure during growth is illustrated by Figure 5.

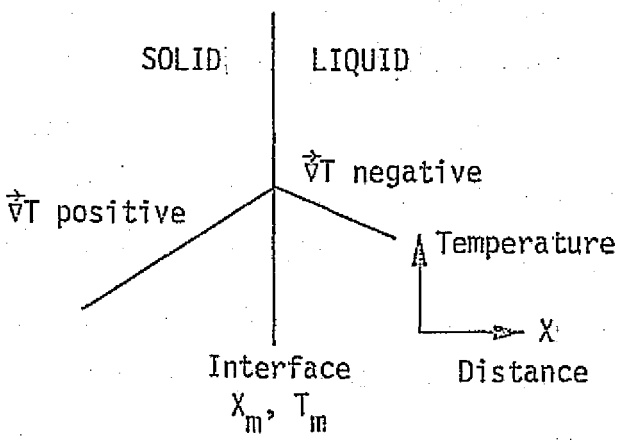

FIGURE 5 THERMAL GRADIENTS AT INTERFACE
(from Reference 16)

When the melt is undercooled, the thermal gradient in front of the interface

$$|\vec{\nabla}| = \frac{T - T_m}{x - x_m} \tag{62}$$

is negative since $T < T_m$. A negative thermal gradient implies a negative gradient of free energy in this region. If an instability occurs in the interface, i.e., the formation of a protuberance, the protuberance would grow into the region of negative $\vec{\nabla}T$ whereas it would merely melt if $\vec{\nabla}T$ were positive. A protuberance which grows becomes a dendrite, and as long as undercooling is maintained in the melt, dendritic growth is sustained. In the case of eutectic alloys, an interface instability also results in lamellar growth. These dendritic or lamellar structures are highly anisotropic, a result which may be desirable or detrimental, depending on the desired application of the resultant solid.

2.2.3 (Continued)

A formal theory of liquid-solid interface stability has been developed by Sekerka [50,51] and extended by Chen [52] to include semi-static external field effects. The geometry of an unstable interface is illustrated by Figure 6 - the dotted line representing a stable, planar interface moving into the liquid with assumed constant velocity V, and the curved line representing a possible shape of an unstable interface in the process of forming a cellular structure in the solid with cells of compositions α and β forming behind the maxima and minima, respectively, of the unstable interface.

It is assumed that the interface is initially planar, and that at some time a small perturbation $\phi(x,t)$ is introduced into the process such that

$$z = \phi(x,t) = \delta(t) \sin \omega x \tag{63}$$

where $\omega = 2\pi/\lambda$ with λ being the wavelength of the perturbation, or the distance over which the concentration varies on a microscopic scale. Obviously, if the perturbation amplitude, δ, increases with time ($\dot{\delta}>0$), the perturbation will grow, the interface will be unstable and the cellular structure, or microsegregation, will result. But if δ does not increase with time ($\dot{\delta}\leq 0$), the interface will remain stable and no microsegregation will occur. So the problem becomes the determination of $\dot{\delta}$ as a function of the solidification parameters, in particular, the solute molecule velocity u and the cell size λ (or ω). u is presumed to be induced by an external field, $\vec{F}$, rather than being due to any internal process, such as Brownian motion.

Calculation of $\dot{\delta}$ is begun by solving the steady state solidification equations

$$\nabla^2 C + \frac{V'}{D} \frac{\partial C}{\partial z} = 0 \tag{64}$$

in liquid

$$\nabla^2 T + \frac{V'}{\alpha_L} \frac{\partial T}{\partial z} = 0 \tag{65}$$

2.2.3 (Continued)

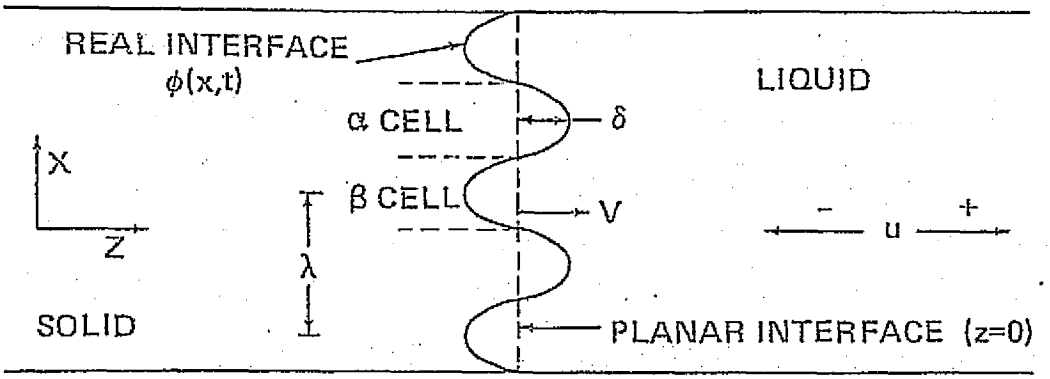

FIGURE 6 INTERFACE GEOMETRY FOR SEKERKA THEORY

$$\text{in solid} \qquad \nabla^2 T' + \frac{V'}{\alpha_s} \frac{\partial T'}{\partial z} = 0 \tag{66}$$

subject to the boundary conditions

$$T_\phi = mC_\phi + T_M \left(1 + \frac{\sigma}{Q} K\right) \tag{67}$$

$$v(x) \equiv V + \dot{\delta} \sin \omega x =$$

$$\frac{1}{Q} \left[K_s \left(\frac{\partial T'}{\partial z}\right) - K_L \left(\frac{\partial T}{\partial z}\right)_\phi\right] =$$

$$\frac{D}{C_\phi (k-1)} \left(\frac{\partial C}{\partial z}\right)_\phi \tag{68}$$

where C is solute concentration, α is thermal diffusivity, m is the slope of the liquidus curve for the system (assumed negative), T_m is the melting temperature, Q is the solvent latent heat of fusion, σ is the interfacial free energy, K is the interface curvature, k is the segregation coefficient ($0<k = C_s/C_L<1$) and $V' = V-u$. The left portion of equation (68) states that the real interface or solidification velocity, v(x) is identically

2.2.3 (Continued)

the sum of the macroscopic planar interface velocity, V, and the time derivative of the small variation from planar geometry, $\phi(x,t)$. The right portion of (68) states that the solidification velocity at each point x on the interface when calculated from heat flow considerations must agree with the velocity calculated from diffusion considerations. The solution for $\dot{\delta}$ obtained from equations (64)-(68) is an extremely complicated function of the parameters listed above as well as the temperature gradients (which are assumed positive) and thermal conductivities in the liquid and solid, the concentration gradient and diffusion coefficient in the liquid and the parameter (V-u/p) where p = 1-k. The sign of $\dot{\delta}$, and thus the occurrence of microsegregation, will depend on the sign of the expression which is obtained for $\dot{\delta}/\delta$

$$\dot{\delta}/\delta = 2\omega(V - \frac{u}{p}) \frac{N(\omega)}{D(\omega)} \qquad (69)$$

where the denominator, $D(\omega)$ and the numerator, $N(\omega)$ both depend on (V-u/p) as well as ω and other "fixed" solidification parameters. Therefore, the solute velocity, which can depend on external fields, enters the determining expression for microsegregation through the term (V-u/p), thus defining the three cases of interest:

$$V - \frac{u}{p} = 0$$

$$V - \frac{u}{p} < 0$$

$$V - \frac{u}{p} > 0 \quad .$$

The analysis which has been performed [52] finds that the interface is stable (no microsegregation) for $V-\frac{u}{p} \leq 0$. When $V-\frac{u}{p} > 0$, the value of $\dot{\delta}$ depends on the relationship of $V-\frac{u}{p}$ to the parameter

$$B \equiv \frac{k\, T_m\, \Gamma V\, V'}{(-m)\, DpC_o}$$

2.2.3 (Continued)

where $\Gamma = \sigma/Q$ and where C_o is liquid concentration in the flat interface case. If $V-\frac{u}{p} \leq B$, the interface remains stable. When $V-\frac{u}{p} > B$, the stability criteria are very complicated [52], but correspond to the stability analysis given by Sekerka [51] if the parameters k and V are redefined as $k' = k\ V/V'$ and $V' = V-u$. Thus for negative m, positive temperature gradients and for $0<k<1$, microsegregation of solute in the solid cannot occur for $V-u/p \leq B$, and for microsegregation to occur when $V-u/p > B$, the system must satisfy the instability criteria described by Sekerka [51].

There remains the question of segregation cell size and its relation to the occurrence of microsegregation. If the entire equation for $\dot{\delta}/\delta$ is plotted versus ω for a given value of V-u/p, curves such as those in Figure 7 result. Curve 1, in which microsegregation is seen to occur,

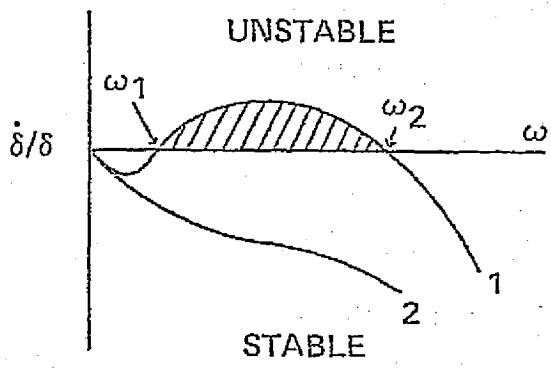

FIGURE 7 SCHEMATIC CURVES OF $\dot{\delta}/\delta$

indicates that the cell size will lie between λ_2 and λ_1 (ω_2 and ω_1). When the tedious calculation is carried out, it is found that the range from λ_2 to λ_1 is on the order of 5×10^{-3} cm, which is in reasonable agreement with experiment [50]. Beyond this order-of-magnitude estimation, further accuracy is impossible because Sekerka's theory is based on (a) steady-state approximations, and (b) assumed small amplitude (linear) perturbations. A transient theory has been

2.2.3 (Continued)

developed [53] to eliminate inaccuracies due to (a), but because of the assumptions in (b), the transient theory does not yield any significant improvement in accuracy. Thus it seems that the indication of the occurrence of microsegregation by the sign of $\dot{\delta}$, and the approach to cell size determination exemplified by Figure 7 constitute the best results available from a theoretical model which describes interface stability and predicts solute distribution characteristics in solids from liquid state parameters.

2.2.4 Gravitational Settling of Nuclei

When a multiphase alloy solidifies in a gravitational field, the settling of nuclei of the heavier phase(s) toward the bottom of the melt results in macroscopic segregation of this solute phase in the solid material. The distribution of nuclei of the heavier phase, C, in the melt should be described by Fick's law

$$D \frac{dC}{dz} = - CU \tag{70}$$

where D is a "nucleus diffusion coefficient", z is the direction of the gravity vector and also the axial direction in an assumed cylindrically shaped melt and U is nucleus settling velocity. The equation of motion for the nucleus, including friction and buoyant forces is thus

$$M \frac{dU}{dt} = Mg - 6\pi\eta rU - \frac{4}{3}\pi r^3 \rho(z) g \tag{71}$$

where M is nucleus mass, r its radius, η the melt viscosity and $\rho(z)$ the melt density (which is assumed to change more slowly with time than U). g is the acceleration due to gravity, 980 cm/sec^2. When equation 71 is solved for U, the result may be written as a function of $\rho(z)$ and g

$$U(z,t) = \left[1 - \frac{\rho(z,t)}{\rho_N}\right] \gamma g D (1 - e^{-t/\gamma D}) \tag{72}$$

2.2.4 (Continued)

where $\rho_N = \frac{3M}{4\pi r^3}$ and $\gamma = \frac{M}{2kT}$. For most reasonable nucleus motion, $t >> \gamma D$, so the exponential vanishes, leaving (for slowly varying melt density)

$$U(z) = \gamma\ g\ D\ [1 - \frac{\rho(z)}{\rho_N}] \quad . \tag{73}$$

Substitution of this result into equation 70 and performance of the integration with respect to z leads to the integral equation

$$\ell n C = - \gamma\ g\ z + \gamma\ g\ f\ (z) \tag{74}$$

where $f(z) = \frac{1}{\rho_N} \int_o^z \rho\ [C(y)]\ dy$ and

$$\rho[C(y)] = \frac{m_1\ C(y) - m_2\ C(y) + m_2\ C_T}{v_1\ C(y) - v_2\ C(y) + v_2\ C_T} \tag{75}$$

with subscripts 1 and 2 referring to solute and solvent atoms, respectively, and C_T being the total (homogeneous) melt concentration or number density. By combining constants, this can be written

$$\rho(C) = \frac{A_3\ C + m'}{A_4\ C + v'} \tag{76}$$

and by noting that equation 74 can be written

$$C = \exp\ [\gamma g\ (f-z)]\ ,$$

one can calculate $\frac{dC}{dz}$ and solve for $\frac{df}{dz}$:

$$\frac{df}{dz} = 1 + \frac{1}{\gamma g c}\ \frac{dC}{dz} \quad . \tag{77}$$

2.2.4 (Continued)

But from the definition of f(z), $\frac{df}{dz}$ is also

$$\frac{df}{dz} = \frac{1}{\rho_N} \frac{A_3 C + m'}{A_4 C + v'} \quad . \tag{78}$$

Equating the right-hand sides of (77) and (78) leads to the new differential equation

$$\frac{(A_4 C + v')\, dC}{B_1 C^2 + B_2 C} = \gamma g z \quad , \tag{79}$$

with

$$B_1 = \frac{A_3}{\rho_N} - A_4 \quad \text{and} \quad B_2 = \frac{m'}{\rho_N} - v' \quad .$$

This can be integrated directly, and applying the boundary condition that $C = C_o$ (the solute concentration equals the homogeneous concentration) at $z = 0$ (the center plane of the melt), the solution obtained is

$$\left(\frac{B_1 C + B_2}{B_1 C_o + B_2}\right)^{\left[\frac{A_4}{B_1} - \frac{v'}{B_2}\right]} \left(\frac{C}{C_o}\right)^{\frac{v'}{B_2}} = e^{\gamma g z} \quad . \tag{80}$$

This is a complicated function of both concentration and melt physical parameters. Therefore its behavior is best illustrated by application to specific problems where all the constants on the left-hand side can be evaluated, as will be done in Section 2.3.2. It should be noted, however, that since the parameter γ depends on the mass and thus the size of the nuclei which are settling, it therefore depends on $(\Delta T)^3$, and adds further complexity to equation 80.

2.2.5 Direct (Non-Convection) Effects of External Fields on Melts

It has been shown [18] that when a liquid is subjected to changes in external fields acting on it, the thermodynamic variables most directly affected are volume and temperature. In particular, if the gravitational field acting on a melt changes by an amount δg, a change in hydrostatic pressure in the melt will result, inducing a corresponding change in specific volume, v, given by

$$\frac{\delta v}{v} = \beta \rho z \delta g \tag{81}$$

where β is the isothermal compressibility, ρ is the density of the melt, and z is the distance below the liquid free surface. The pressure change also induces a temperature change given by

$$\delta T = \frac{\delta v}{\alpha v} = \frac{\beta}{\alpha} \rho z \delta g \tag{82}$$

where α is the thermal expansion coefficient. Other variables affected by a field change through their dependence on volume or temperature include: diffusion coefficient, Gibbs free energy, and interfacial energy, if σ is dependent on T in the first place. More complicated parameters, such as nucleation rate, nucleus radius, solidification rate, total solidification time and grain size depend on combinations of the above variables. The heterogeneous nucleation rate is one of the most important parameters affected by field changes, and the calculation of the altered nucleation rate, I', is greatly simplified if the interfacial energies are not influenced by field changes - that is, if σ does not depend strongly on temperature. The problem can be illustrated by recalling that I is an exponential function of $f(\theta)$ where

$$f(\theta) = \frac{1}{4} (1-\cos \theta)^2 (2+\cos \theta)$$

and

$$\cos \theta = \frac{\sigma_{s\ell} - \sigma_{ns}}{\sigma_{\ell n}}$$

2.2.5 (Continued)

where the subscripts s, ℓ and n refer to substrate, liquid and nucleus, respectively. If σ_{ij} is a function of T, and therefore, under changed field conditions, of δT, the difficulty of calculating $I'(\delta T)$ over calculating I' for constant $f(\theta)$ or fixed σ_{ij}, is obvious. At present there is no experimental evidence and no theoretical justification, other than Spaepen's work [34], for considering σ or σ_{ij} to be more than very weakly dependent on temperature.

In general, the effect which external field changes have on physical properties of melts, such as those listed above, may be found by replacing T and ν in the equations for the properties of interest with T' and ν', where the primes refer to the values of the variables in the changed field:

$$T' = T + \delta T \tag{83}$$

and

$$\nu' = \nu + \delta\nu \quad . \tag{84}$$

The field effect on undercooling is thus

$$\Delta T' = T_M - T' = T_M - T - \delta T = \Delta T - \delta T \quad . \tag{85}$$

Hence the undercooling is decreased by a positive δT and enhanced by a negative δT. It should be noted that free energy calculations require more knowledge of the field conditions than is contained in equations 83-85, due to the direct dependence on pressure. Also, equations 81 and 82, as they are written, hold only for gravity field changes. For magnetic fields, the corresponding equations are [18]

$$\frac{\delta\nu}{\nu} = \frac{1}{2} \beta \mu_o (H_o^2 - \chi H^2) \tag{86}$$

2.2.5 (Continued)

and

$$\frac{\delta T}{T} = \frac{1}{4} (\chi_\ell - \chi_s) \frac{H^2}{Q} \tag{87}$$

where μ_o is the permeability of free space, χ is magnetic susceptibility, H_o is the initial and H the final field strength in the liquid, and Q is heat of fusion.

2.2.6 The Relation of Solid Physical Properties to Structure and Electron and Phonon Scattering

The influence of undercooling, nucleation and general solidification history on the physical properties of materials solidifying from the melt was investigated as part of the attempt to understand how all solid properties might be better predicted and controlled by manipulation of the solidification process. It appears that no direct link exists between the solidification process and the physical properties of the resultant solid. However, the two are linked through the structural nature of the solid which depends directly on solidification history, primarily the undercooling and nucleation of the melt. Many physical properties of solids, such as thermal conductivity, electrical resistance, Grüneisen parameter, and specific heat depend on the scattering of electrons and phonons by non-periodic structures in the solid. In particular, three physical properties of solids, the thermal conductivity, κ, the electrical conductivity, σ, and the thermoelectric power, Q', have been found to depend on the phonon mean free path, Λ, in the solid. Specifically the relationships are given by Ziman [54,55] as:

$$\kappa = \frac{1}{3} \bar{v} \, c \, \Lambda \tag{88}$$

$$\sigma = \frac{3e^2}{\pi^2 k^2 T} \kappa \tag{89}$$

$$Q' = \frac{1}{eK_3} \left(\frac{K_4}{T} - \kappa\right) \tag{90}$$

2.2.6 (Continued)

with K_3 and K_4 being the magnitudes of the tensor transport coefficients

$$\overleftrightarrow{K}_0 = \frac{1}{4\pi^3/n} \int \Lambda_e \frac{\vec{v}\,\vec{v}}{v\,v} dS_F \tag{91}$$

$$\overleftrightarrow{K}_3 = \frac{1}{3} \pi^2 (kT)^2 \left[\frac{\partial}{\partial \varepsilon} \overleftrightarrow{K}_0 (\varepsilon)\right]_{\varepsilon=\mu} \tag{92}$$

$$\overleftrightarrow{K}_4 = \frac{1}{3} \pi^2 (kT)^2 \overleftrightarrow{K}_0 (\mu) \tag{93}$$

where $\bar{v}$ = average phonon velocity in the solid
c = heat capacity
e = electronic charge
dS_F = differential of the Fermi surface
T = absolute temperature
$\vec{v}$ = velocity of the electron or hole carrier
v = $|\vec{v}|$
Λ_e = electron mean free path in the solid

and μ is the free energy of an electron, i.e., its chemical potential. Ziman also reports [55] that the phonon mean free path in polycrystalline solids is on the order of the size of the grains. That is,

$$\Lambda_i \simeq \sqrt[3]{v_g^i} \tag{94}$$

where v_g^i is the volume of the i^{th} crystal grain. Thus grain size in a polycrystalline solid can be expected to have some effect on the thermal conductivity of the solid, and through κ, on σ and Q' as well. This effect is usually masked by the considerable temperature dependence of κ through c. As is well known, structural properties such as strength, hardness and plastic deformation are more directly related to solid structure and hence to the solidification process. The relationship of the solidification environment and process to structural and physical properties is illustrated by Figure 8.

2.2.6 (Continued)

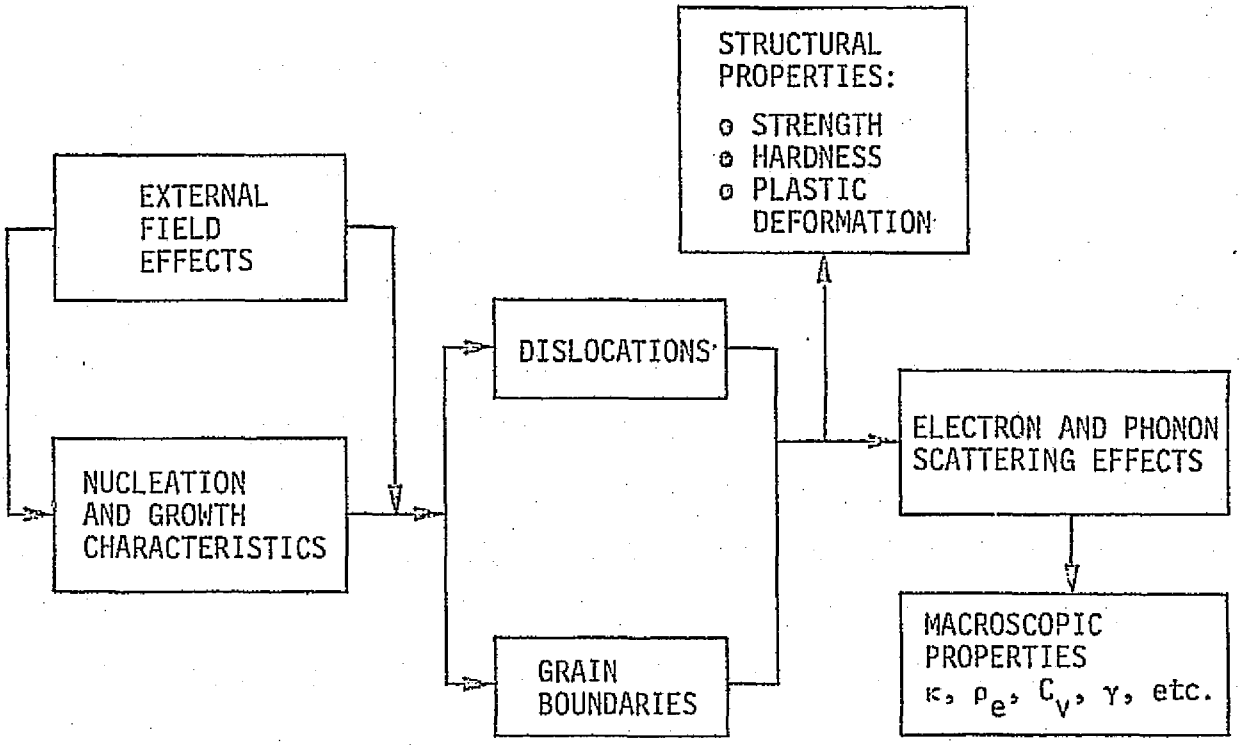

FIGURE 8 HYPOTHETICAL RELATION OF SOLIDIFICATION PROCESSES TO PHYSICAL PROPERTIES

2.2.7 A Solidification Model to Predict Grain Size and Dendrite Morphology

For a long time, it has been known empirically that grain size in a polycrystalline solid depended on solidification history, primarily on undercooling. More recently, it was shown experimentally [56] that the morphology of dendrites also depends on these processes. If the proper mathematical relationships between nucleation and growth of crystalline grains from the melt can be found, and if the proper external boundary conditions can be applied, then in principle it should be possible to predict something of a solid's structure from a knowledge of the melt properties and environment. An attempt to develop such a predictive model will now be described.

2.2.7 (Continued)

Kattamis and Flemings [56] reported observing a distinct change in dendrite morphology as a function of melt undercooling. To describe this theoretically, a "morphology parameter" may be defined, which is simply the ratio of that portion of a dendrite's volume due to growth, v_g, to the portion which nucleates initially, v_n. Figure 9 shows a cylindrical dendrite growing from a spherical cap nucleus formed on a heterogeneous nucleant substrate, characterized by wetting angle θ.

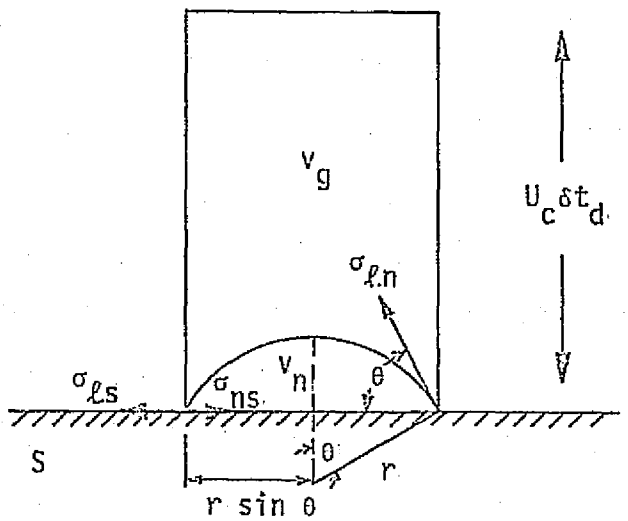

FIGURE 9 SIMPLE DENDRITE - NUCLEUS MODEL

As was shown in Section 2.1.3, the nucleus volume is given by

$$v_n = \frac{4}{3} \pi r^3 f(\theta) \quad . \tag{95}$$

The area of the dendrite base is that of the nucleus and is simply $\pi r^2 \sin^2\theta$. To a close approximation, the dendrite length will be the product of the growth rate, U_c, with the growing time, δt_d, which is the time required for solute atoms to diffuse from the extremities of the region in which a dendrite is growing to the tip of the dendrite. Hence

$$v_g = \pi r^2 \sin^2\theta \; U_c \; \delta t_d \quad . \tag{96}$$

2.2.7 (Continued)

Now r depends on undercooling via equation 19, $f(\theta)$ and $\sin^2\theta$ depend on the nucleant, U_c is a function of undercooling through equations 60 and 61, and δt_d is given by

$$\delta t_d = \sqrt{\frac{M}{T}} \left(\frac{V}{N}\right)^{1/3} \tag{97}$$

where $\frac{V}{N}$ is the volume of a grain and

$$M = \frac{\pi\, m\, \rho_s a^3}{48\, k}$$

with m = solute atom mass
ρ_s = solute atom density
a = solute atom radius
k = Boltzmann's constant.

The total volume of material, V, is assumed known, so the remaining unknown is N, the total number of nuclei which form in the melt. This number is

$$N = I\, V\, \delta t_h \tag{98a}$$

or the grain size is

$$\frac{V}{N} = \frac{1}{I \delta t_h} \tag{98b}$$

where I is nucleation rate (equations 1 and 20) and δt_h is the time required for heat to flow out of that region of the melt where a single nucleus is forming and is expressed by

$$\delta t_h = \left(\frac{V}{N}\right)^{2/3} \frac{\sqrt{3}}{2\alpha_T} \tag{99}$$

where α_T is the thermal diffusivity of the melt. In this first attempt at development of a predictive solidification model, equations 97 and 99, the diffusion and heat flow constraints, are derived by dividing the melt

2.2.7 (Continued)

into N imaginary cubes. One nucleus is assumed to form at the center of each cube at some time during the interval $\delta t_h > \delta t_d$, which is taken as the total solidification time. The maximum distance which either a solute molecule or heat must travel is that distance from the center of the cube to a corner, $\sqrt{\frac{3}{2}}(\frac{V}{N})^{1/3}$. Dimensional analysis of the fundamental diffusion and heat flow equations then leads to equations 97 and 99.

Equations 95 through 99 plus 1, 19, 20, 60 and 61 may be solved simultaneously (a Wang 700A computer program has been developed for this purpose) to yield values of all unknown parameters, particularly the morphology, v_g/v_n, and the grain size, $\frac{V}{N}$. Of course $\frac{V}{N}$ is really the size of each imaginary cube, but its value gives a reasonable indication of average grain size in the solid and $(\frac{V}{N})^{1/3}$ is an order of magnitude estimate of dendrite spacing. There are three value ranges of v_g/v_n which are of interest, each corresponding to a morphology observed by Kattamis and Flemings, and shown in Table II.

TABLE II DENDRITE MORPHOLOGY CORRELATION

Value of v_g/v_n	Dendrite Morphology
>> 1	normal
≈ 1	cylindrical
<< 1	spherical

This crude first cut at a mathematical model to calculate grain size and morphology in solids from solidification history contains several simplifying assumptions or deficiencies which should be remedied by more rigorous analyses. The most obvious of these are:

1. No account is taken of dendrite branching (other than as a heterogeneous nucleation site for a new dendrite) or of the limiting of one dendrite's growth by other dendrites (except to limit each dendrite to its cube).

2.2.7 (Continued)

2. The heat flow constraint treats only the local (cube) thermal environment, and treats each cube independently; total melt heat transfer analysis is required.

3. A better definition of total solidification time is required.

4. Model accuracy is no better than the "constant" input parameters used for numerical calculation. At present, very few of the properties of melts required by this model are known with any accuracy.

Although these obstacles are formidible, calculations can be made with the present model which are accurate enough to at least allow comparison with experiment, as is done in Section 2.3.3. The reason for pursuing development of this model is clear: it forms the core of a much larger model whose purpose is nothing less than complete analytical materials design for user requirements, using gravity, or microgravity, as a primary variable. Such a model will be discussed in Section 2.4.1.

2.3 APPLICATION OF THEORY TO EXPERIMENTAL PROBLEMS

2.3.1 Undercooling and Growth of NH_4Cl-H_2O in Microgravity

Two solidification experiments with the metal-model material NH_4Cl-H_2O (ammonium chloride solution) have been flown by Johnston and Griner of MSFC in the Space Processing Applications Rocket (SPAR) experiment program. The December, 1975 flight experiment sample began to solidify at a known growth rate, and it was useful to calculate the undercooling corresponding to that growth rate. The May, 1976 flight experiment sample undercooled a known amount, but failed to solidify. Appropriate portions of the theory from Sections 2.1 and 2.2 were applied to these experiments to provide further insight into what occurred experimentally.

In order to perform calculations of nucleation and growth rates, it is necessary to have values of melt parameters such as entropy of fusion, S_c, liquid-solid interfacial energy, σ, and diffusion coefficient, D. Unfortunately, none of these values is known for NH_4Cl-H_2O. However, being a metal-model material, it will have values of S_c, σ and D which are approximately in the range common to most metals. In particular, most metals have a value of S_c which is, within about 50%, equal to Boltzmann's constant, $8.3167 \times 10^7 \frac{erg}{mole\ °K}$. Turnbull [4] has shown empirically that a reasonable approximation for σ can be derived from the value of S_c by the relation

$$\sigma \cong \frac{.45\ S_c T_m}{N^{1/3}\ v^{2/3}}$$

where T_m is the equilibrium melting temperature, N is Avogadro's number and v is the specific volume. For the ammonium chloride solution used (28% by weight NH_4Cl), the known parameters are

$$T_m = 295.8\ °K$$
$$v = 6.68\ cm^3/mole\ .$$

Using this information, the interfacial energy was found to be 37 erg/cm^2. Since the diffusion coefficient for most metals is near 4×10^{-5} cm^2/sec,

2.3.1 (Continued)

this leads to a value for A_2/A_1 in equations 60 and 61 of 0.0036 cm/sec°K^2. If one writes the heterogeneous nucleation rate equation (see equations 1 and 20) as

$$I = \exp\left[75.985 - \frac{A^2 f(\theta)}{(T_m - \Delta T)\ \Delta T^2}\right] \qquad (100a)$$

the value of A^2 obtained with the above values of the NH_4Cl-H_2O parameters is 39.665 X 10^6 °K^3.

December 1975 SPAR Experiment

Since the growth rate was observed to be 0.018 cm/sec (1.08 cm/min) in this experiment, the problem was to determine the probable amount of undercooling causing this rate. This was done by using equation 60

$$U_c = \left(.0036 \frac{cm}{sec\ °K^2}\right) \Delta T^2$$

to calculate the curve shown in Figure 10. As seen from this curve, the undercooling value corresponding to 1.08 cm/min growth rate is 2.25°K. Metal values of D and S_c do not vary much from those assumed above, so the product $D\ S_c^2$ will probably not affect the calculated value of undercooling. However, σ can vary from about 25 erg/cm^2 to 300 erg/cm^2, which leads to the following spread in calculated undercooling values for NH_4Cl-H_2O:

$$1°K < \Delta T < 4°K \quad .$$

Thus the undercooling, though quite small, was sufficient to initiate solidification in the sample in the time available on the rocket flight.

May 1976 SPAR Experiment

In this experiment, good temperature versus time flight data curves were obtained, but the sample failed to solidify. For the purpose of calculation, time data read from these curves is presented (for each

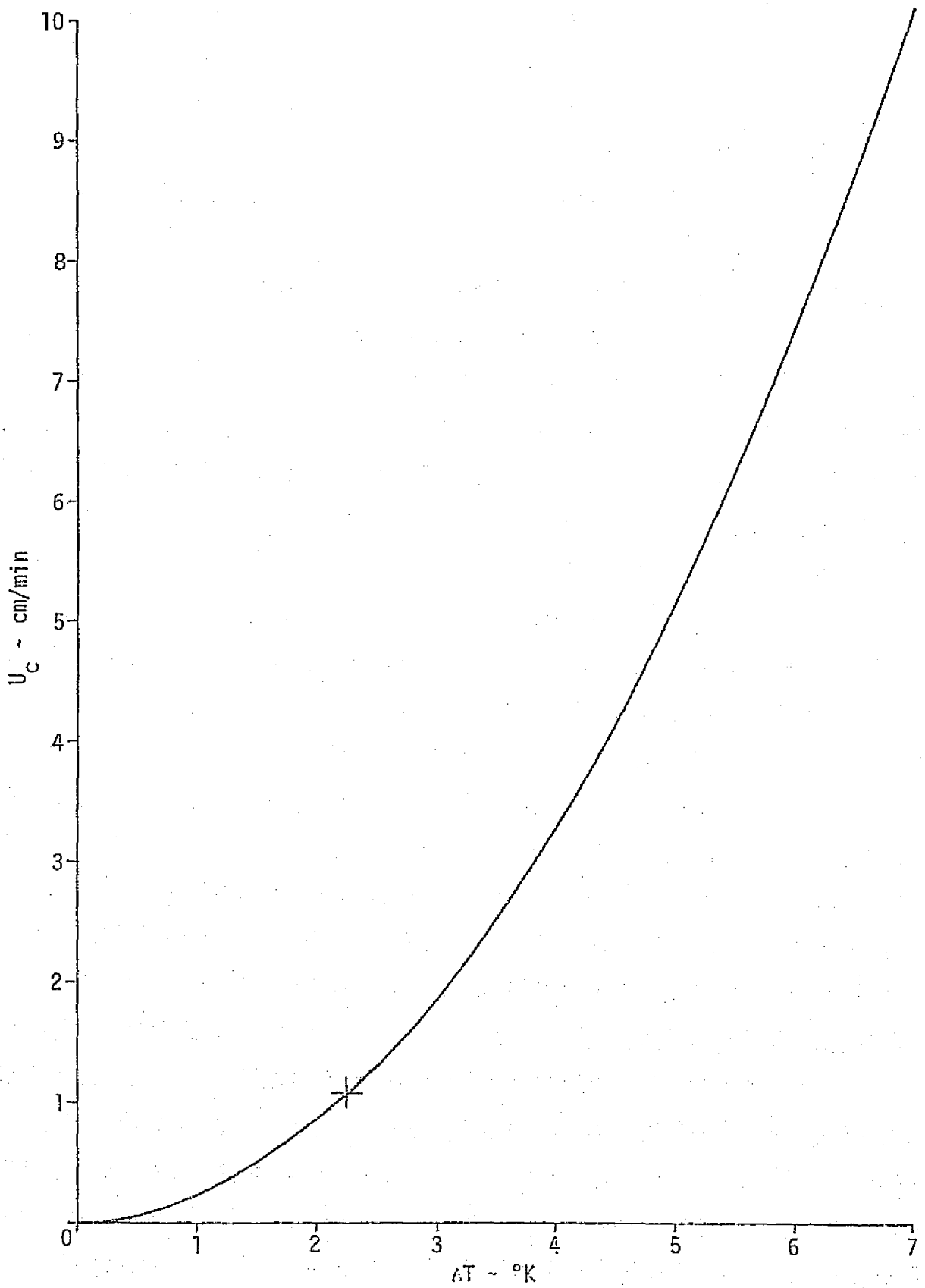

FIGURE 10 GROWTH RATE VS. UNDERCOOLING FOR AMMONIUM CHLORIDE SOLUTION

2.3.1 (Continued)

thermistor) in Table III as the "time during which the sample region measured by a given thermistor was below the value of undercooling shown in column 3". Since the sample was approximately 5 cm long by 1 cm^2, a minimum allowable growth rate to solidify in the available time can be estimated. The growth rate calculated from the undercooling is shown in column 5, and the time required to solidify the sample at that growth rate is in column 6. This data indicates that there was

TABLE III MAY '76 SPAR NH_4Cl EXPERIMENT DATA

Thermistor	Time Sec.	ΔT °k	Min. U_c cm/sec	U_c cm/sec	Time to Solidify sec
1	250	6.8	.02	.167	30
2	sample heated	---	---	---	---
3	200	5.8	.025	.122	41
4 & 5	240	17.8	.021	1.146	4.4
6	sample heated	---	---	---	---
7	195	7.8	.0256	.22	23

sufficient time for solidification if nucleation had occurred. The fact that nucleation did not occur at the undercooling measured by the thermistors, while it did occur at lower undercooling in the December experiment, indicates that certain "low angle" heterogeneous nucleating agents were destroyed in the melt prior to launch, i.e., the sample was "denucleated". This statement can be quantified if equation 100a is solved for f(e),

$$f(\theta) = [75.985 - \ell n\ I]\ \frac{(295.8-\Delta T)\ \Delta T^2}{39.665 \times 10^6} \qquad (100b)$$

values of nucleation rate are assumed, and a table of values of e versus f(e) is available. Turnbull [7] defines a "measurable" nucleation rate as

$$1\ \frac{\text{nucleus}}{cm^3 sec} < I < 10^6\ \frac{\text{nuclei}}{cm^3 sec}\ .$$

2.3.1 (Continued)

To assure not only measurable nucleation rates but solidification of the sample within the time available, values for I of 10^2 to 10^8 nuclei/cm^3sec were substituted in equation 100b to produce the curves in Figure 11. For such a large variation in I, the band separating the two regions indicated is quite small. Since nucleation did not occur in this experiment, and undercoolings of up to 17.8°K were obtained in some regions of the sample, it is clear that nucleants characterized by wetting angles of up to 60° were dissolved into the melt, i.e., denucleated. As used here, the wetting angle, θ, is a convenient parameter for characterizing heterogeneous nucleants, and is not necessarily a strict physical quantity. If this were so, every nucleus that formed would have to be a spherical cap on a planar impurity particle substrate. While this probably occurs some of the time, assuming that all nuclei form this way is unjustified.

That all nucleants with wetting angles lower than 60° were denucleated is indicated by the fact that if a nucleus had formed in the melt region where ΔT = 17.8°K, its growth rate, although slower in other parts of the melt as shown in Table III, would still have been sufficient to solidify the sample. That nucleants of angles up to 60° were denucleated only in that one highly undercooled region but still existed elsewhere in the melt is most unlikely. If nucleants characterized by wetting angles of around 62° or more were still active in the melt, a sustained undercooling of more than 21°K would have been required, according to Figure 11. The melt regions around thermistors 4 and 5 attained this undercooling for about two minutes, indicating that even these nucleants had been denucleated.

2.3.2 Undercooling and Nucleation of Lead-Tin Eutectic Material in a Centrifuge

Effects of undercooling and gravity on solidifying materials were studied in a series of experiments on Pb-Sn eutectic material by Johnston and Griner at MSFC [57]. This material was selected for the drastic difference

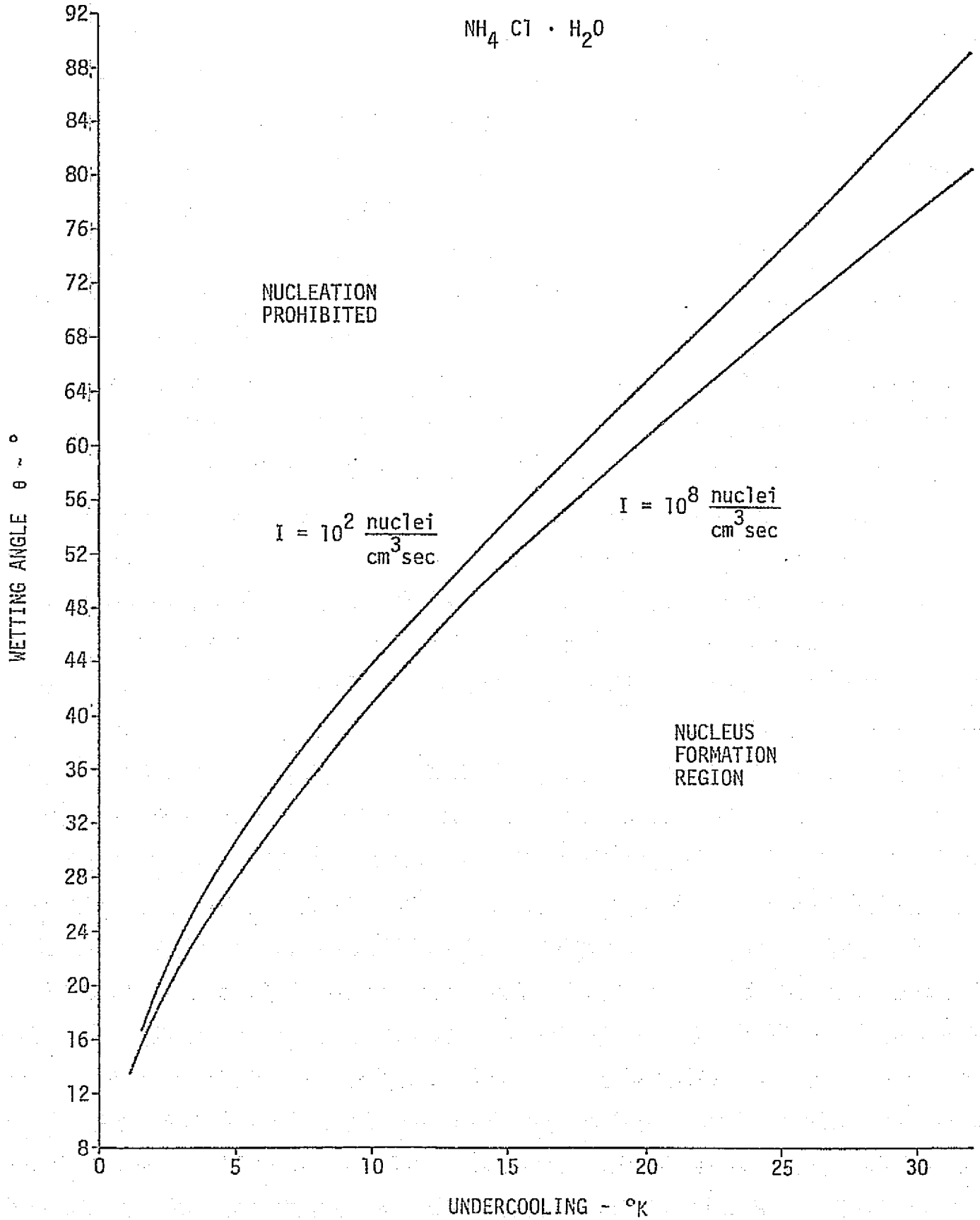

FIGURE 11 NUCLEANT WETTING ANGLE VS. UNDERCOOLING REQUIRED FOR SOLIDIFICATION

2.3.2 (Continued)

in density of its components. In the experiments, initially solid samples of eutectic composition (X = 26 atomic % Pb) were melted in a 1.5 cm long by 1.2 cm diameter cylindrical crucible, and held in the molten state while inside a centrifuge providing a fixed centripetal acceleration equal to some integral multiple of g, 980 cm/sec^2. The samples were then cooled, solidified, removed from the crucible and analyzed metallographically to determine the volume fraction of Pb-rich dendrites at the bottom of the sample. Table IV presents the results of these experiments, along with the conversion of the volume fraction, V_v, to total lead atomic fraction through the Pb atomic fraction in the dendrites, X^D. X^D was obtained from an approximation of the Pb-Sn phase diagram in the temperature-concentration region of interest, shown in Figure 12. The value of component concentration is related to atomic fraction by

$$X = C/C_T \tag{101}$$

where C_T is total melt concentration. Any concentration value is computed from

$$C_i = N_o \frac{\rho_i}{M_i} \tag{102}$$

where N_o is Avogadro's number, ρ_i is density of the i^{th} component and M_i is its atomic weight. For the Pb-Sn eutectic melt, the following values were calculated

$$C_T = 0.35802 \times 10^{23} \text{ cm}^{-3}$$

$$C_o^{Pb} = 0.1038 \times 10^{23} \text{ cm}^{-3} \quad .$$

After obtaining other melt parameters, the constants in equation 80 can be evaluated as follows

$$v' = v_{Sn} C_T = 0.96486$$

$$m' = M_{Sn} C_T = 7.053 \text{ gm/cm}^3$$

TABLE IV MSFC CENTRIFUGE EXPERIMENT DATA

SAMPLE	g LEVEL	ΔT, °K	V_v, %	Pb CONCENTRATION IN DENDRITES, X^D	TOTAL Pb CONCENTRATION ATOMIC %
2A1	1	0	27	.710	38
3A1 ⊙	1	7.5	35	.733	43
5A1	1	8.6	37	.737	44
1A1	1	11.34	40.5	.745	46
1A3	3	0	46.5	.710	47
2A3	3	6.05	49.5	.728	49
--- △	3	10.8	--	.743	--
3A3	3	11.34	56.5	.745	53
5A3	3	14.7	59	.755	55
4A5	5	0	50	.710	48.5
3A5	5	1.89	--	.715	--
2A5	5	6.05	55.5	.728	52
1A5 ⊡	5	7.0	--	.762	--
5A5	5	8.69	60	.737	55
7A5	5	16.44	45.5	.760	49

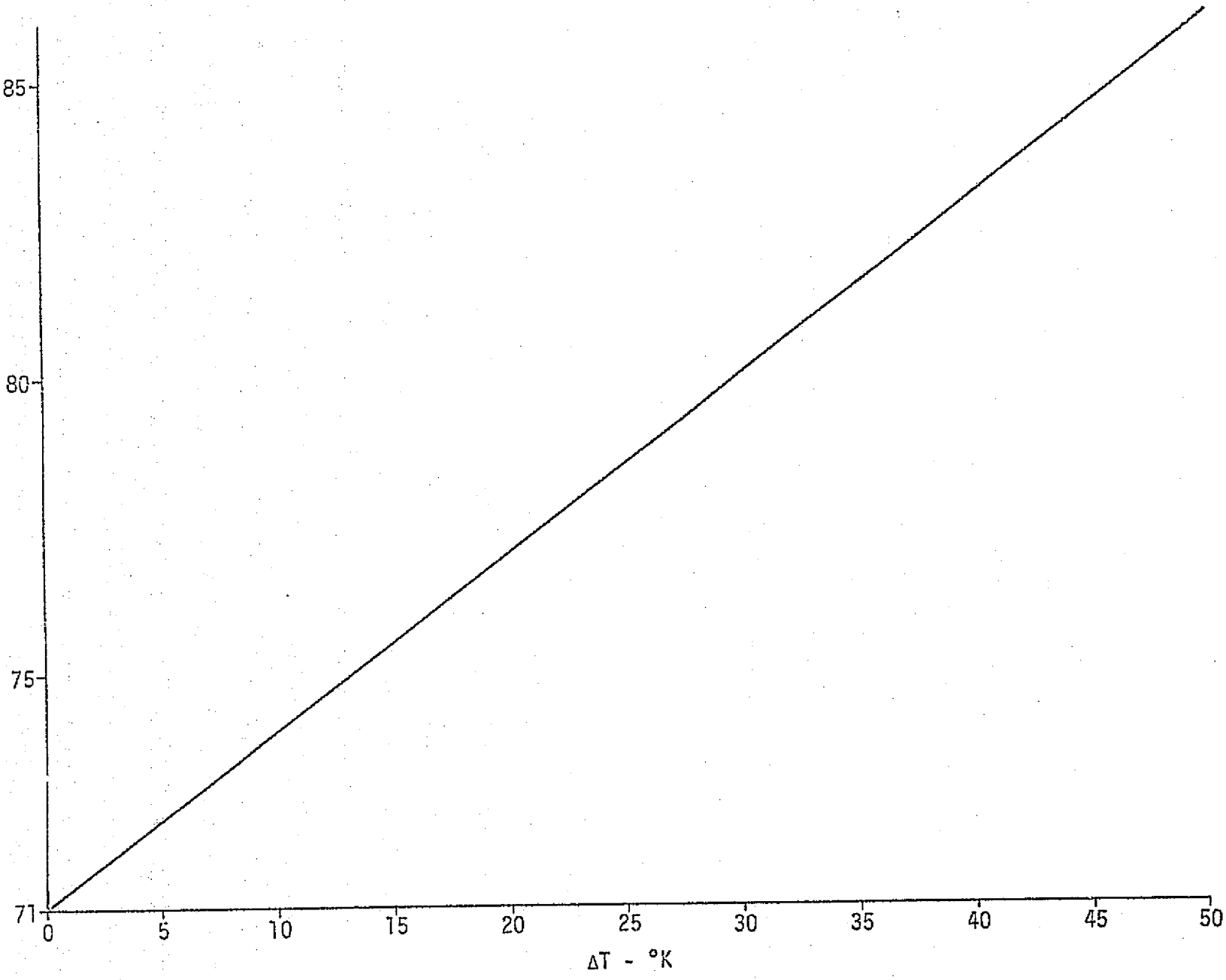

FIGURE 12 APPROXIMATE ATOMIC % Pb IN DENDRITES THAT NUCLEATE AT ΔT

2.3.2 (Continued)

$$A_4 = v_{Pb} - v_{Sn} = 0.335 \times 10^{-23} \text{ cm}^3$$

$$A_3 = m_{Pb} - m_{Sn} = 14.69 \times 10^{-23} \text{ gm}$$

$$B_2 = m'/\rho_N - v' = -0.3442$$

$$B_1 = A_3/\rho_N - A_4 = 0.9577 \times 10^{-23} \text{ cm}^3$$

$$v'/B_2 = -2.8$$

$$A_4/B_1 = 0.35 \quad .$$

Equation 80 now becomes

$$\left[\frac{(.9577 \times 10^{-23})\, C - .3442}{-0.24479}\right]^{3.153} \left(\frac{.1038 \times 10^{23}}{C}\right)^{2.803} = e^{\gamma g z} \quad . \qquad (103)$$

Since the parameter γ depends on the mass and thus the size of the nuclei which are being segregated, it therefore depends on the cube of the undercooling, ΔT. Thus to calculate the lead distribution in a sample of size $-.75 \text{ cm} < z < +.75 \text{ cm}$ (as shown in Figure 13), particular values of both ΔT and g must be specified. If a value of 10°K is chosen for ΔT, curves for lead concentration distribution for different gravity levels, as shown in Figure 14, are generated by equation 103. Since concentration was measured at only one position ($z = -0.75$) for the MSFC samples, no comparison between theory and the MSFC experiment can be made. However, Strangman and Kattamis [58] performed a similar experiment (at 1-g) and their data is provided for comparison on the right side of Figure 14.

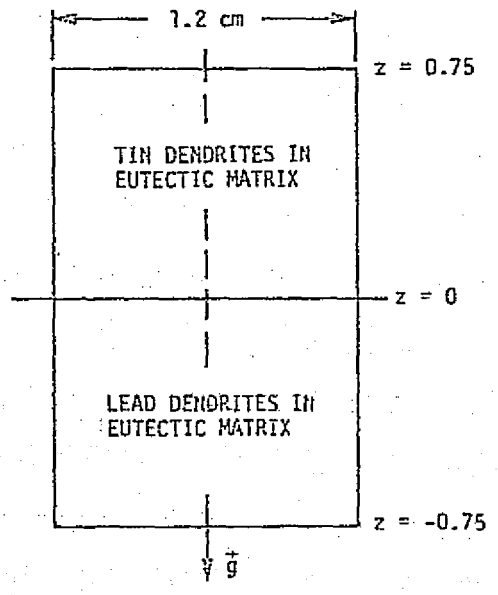

Figure 13 SAMPLE COORDINATE SYSTEM

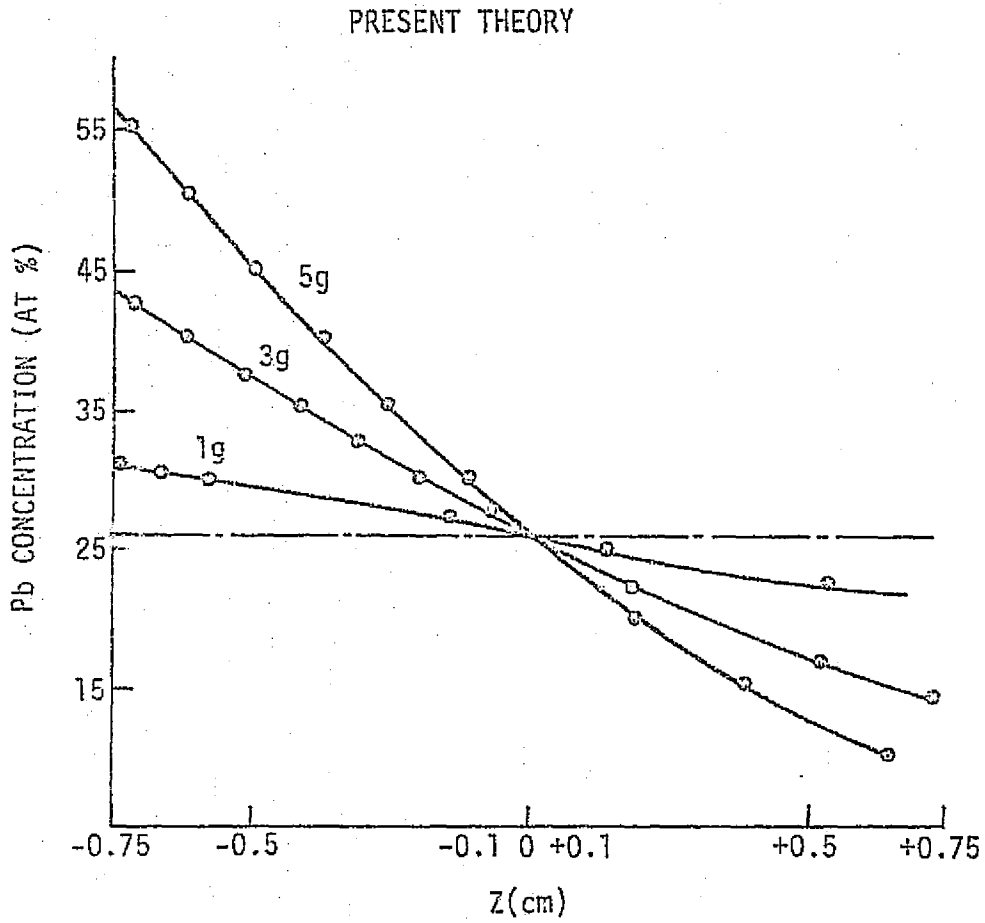

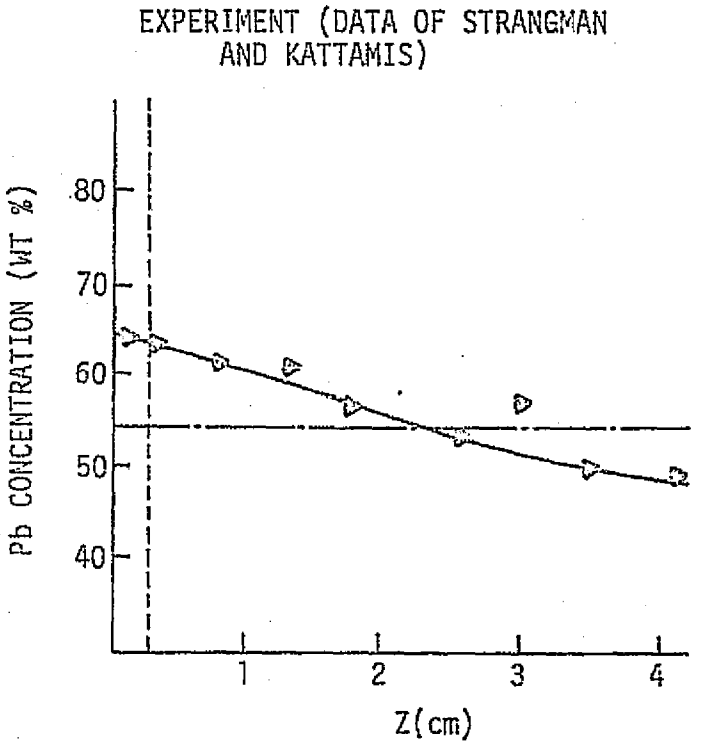

FIGURE 14 CONCENTRATION VS. POSITION

2.3.2 (Continued)

Their material was of a different starting composition from the MSFC samples, complicating comparison. Qualitatively, agreement is good.

The most direct comparison between theory and the MSFC experiments is shown in Figure 15. Here atomic fraction is plotted versus gravity for a ΔT of 10°K at a position of $z = -0.75$. Although three data points are not really sufficient to define a curve, it is clear that the position and slope of any curve through the experimental points would be quite different from those of the theoretical curve. This difference is attributed to the roughly linear increase in segregation with undercooling exhibited by the original data (Table IV and [57]), and not accounted for by the ΔT dependence of γ in equation 103.

The hypothesis that observed Pb dendrite segregation is the result of nuclei transport in the melt during a transport time, t_t, which is a function of undercooling and during which time the entire melt is undercooled, was tested by estimating the time required for a nucleus moving with velocity

$$U = g\gamma D \left[1 - \frac{\rho(z)}{\rho_{Pb}}\right] \tag{104}$$

to travel a distance of 0.75 cm. The relation of t_t to the rest of the solidification cycle is shown in Figure 16. For Pb nuclei of mass on the order of 10^{-16} gm,

$$\gamma D = \frac{M D}{2kT} \approx 2.4 \times 10^{-8} \text{ sec} \quad . \tag{105}$$

Thus

$$t_t = \frac{.75 \text{ cm}}{U} \approx \frac{3 \times 10^7}{g[1-\rho(z)/\rho_{Pb}]} \quad . \tag{106}$$

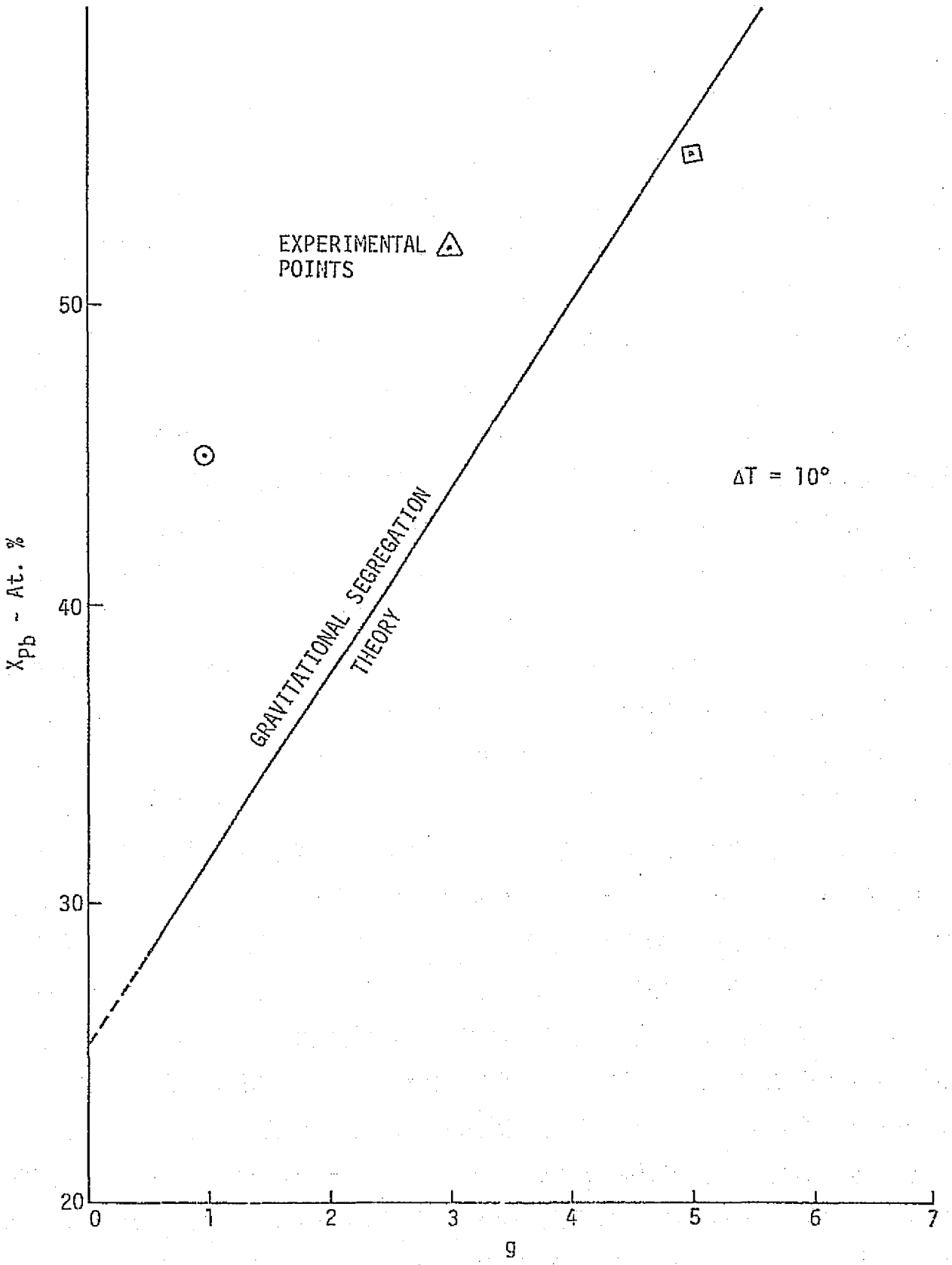

FIGURE 15 GRAVITATIONAL SEGRECATION OF LEAD IN LEAD-TIN EUTECTIC ALLOY

2.3.2 (Continued)

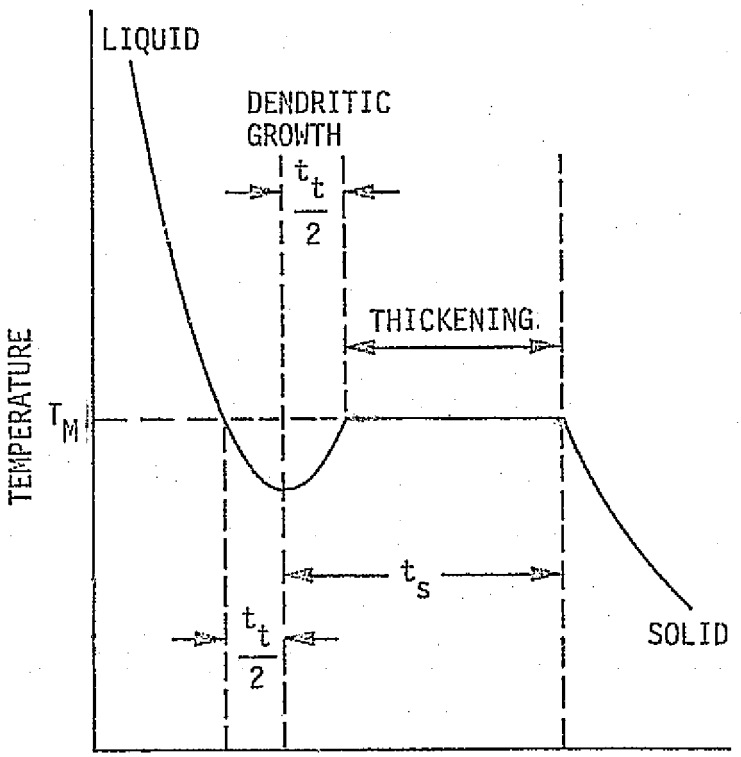

FIGURE 16 SOLIDIFICATION CYCLE

For nominal values of g and D, the smallest values of t_t will be for the case of $\rho(z)/\rho_{Pb} << 1$. Even then, t_t is on the order of 10^4 sec. Since t_s is known experimentally to be about 10 sec. to 60 sec. depending on g level and undercooling, t_t must be on the order of 10^1 sec. This discrepancy invalidates the original hypothesis, if the assumed magnitude of 10^{-5} cm^2/sec for the "transport coefficient", D, is correct for nuclei this large.

Thus the mechanism by which undercooling produces the non-gravity-related segregation of Pb dendrites observed in the MSFC centrifuge experiments remains a mystery. In fact, the observed increase in segregation with increase in undercooling seen in Table IV, is contrary to all explanations of melt dynamics considered in this study. More effort will be required to explain this anomalous effect.

2.3.3 Morphology and Grain Size of Fe-.25 Ni Alloy

As mentioned in Section 2.2.7, Kattamis and Flemings [56] performed the experimental work which established the effect of undercooling on dendrite morphology and grain size. They worked with several alloys, but one which they studied most extensively was Fe-.25Ni. As so happens, the elements Fe and Ni are also two of the few elements, solid at STP, for which all the melt properties required by the mathematical model of Section 2.2.7 are either known or can be deduced. Hence this was the material chosen for comparison between theory and experiment.

The first step was to evaluate all the constants required by the model equations. Using values of the element properties given in Table VII for iron and nickel, values of the constants were computed from their defining equations. Some of the constants pertain only to the solvent or solute, and evaluation is straightforward. In cases where the constant pertains to the melt as a whole, the melt properties of interest, y, were estimated from the expression

$$y = .75y_{Fe} + .25y_{Ni} \tag{107}$$

where y_{Fe} and y_{Ni} refer to the property for pure iron or nickel.

Although this expression probably does not accurately represent many alloy melt properties, it does represent some, and it is the only means at present of obtaining those properties not specifically measured. The form of the model equations used was as follows:

Nucleus Volume: $$v_n = \frac{4}{3}\pi r^{*3} f(\theta) = \gamma_1 \frac{f(\theta)}{\Delta T^3} \tag{108}$$

Dendrite Growth Volume: $$v_g = \frac{\pi}{2} r^{*2} \sin^2\theta\, U_c\, \delta t_d = \gamma_2 \sin^2\theta \frac{\delta T_d}{T} \tag{109}$$

Growth Rate: $$U_c = \frac{vDS_c^2}{4\pi\sigma kT} \Delta T^2 \tag{110}$$

Nuclei Creation: $$N = I\, V\, \delta t_h \tag{111}$$

2.3.3 (Continued)

Nucleation Rate: $$I = \exp\left[75.985 - \frac{A^2 f(\theta)}{T\,\Delta T^2}\right] \quad (112)$$

Nucleus Radius: $$r^* = \frac{2\sigma}{S_c \Delta T} \quad (113)$$

Solute Diffusion Constraint: $$\delta t_d = \left(\frac{V}{N}\right)^{1/3} \sqrt{\frac{M}{T}} \quad (114)$$

Heat Flow Constraint: $$\delta t_h = \left(\frac{V}{N}\right)^{2/3} \frac{\sqrt{3}}{2\alpha_T} \quad (115)$$

Grain Dimension or Dendrite Spacing: $$\ell = \left(\frac{V}{N}\right)^{1/3} = \left(\frac{2\alpha_T}{3I}\right)^{1/5} \quad (116)$$

with the constants being

$$\gamma_1 = \frac{32}{3} \pi \left(\frac{\sigma}{S_c}\right)^3 = 1.603 \times 10^{-13}\ \text{cm}^3\ ^\circ\text{K}^3$$

$$\gamma_2 = \frac{vD\sigma}{2k} = 4.2446 \times 10^{-10}\ \frac{\text{cm}^3\ ^\circ\text{K}}{\text{sec}}$$

$$A^2 = \frac{16\ \pi\ \sigma^3}{3\ k\ S_c^2} = 7.469 \times 10^9\ ^\circ\text{K}^3$$

$$M = \frac{\pi}{48k} \rho_{Ni} a^3 = 1.85019 \times 10^{-9}\ \frac{\text{sec}^2}{\text{cm}^2}\ ^\circ\text{K} \quad .$$

The equations of the model (108-116) may now be solved simultaneously using the above constants and assumed values for the independent variables, θ and ΔT. Table V was constructed to provide input values of $f(\theta)$ and $\sin^2\theta$, and a Wang 700A computer program was written to facilitate calculation of several solid quantities (such as morphology parameter, v_g/v_n; dendrite arm spacing, ℓ; total dendrite volume, $v_{dendrite} = v_g + v_n$; and grain size, $\frac{V}{N}$) as a function of a wide range of wetting angle and undercooling. Table VI presents the results of such a calculation for the critical region for the Fe-.25N_i alloy of θ=81° and 148°K < ΔT < 200°K. Kattamis and Flemings had reported a sharp transition from cylindrical to spherical morphology at ΔT = 170°, hence the interest in this region.

TABLE V FUNCTIONS OF NUCLEANT WETTING ANGLE

θ	f(θ)	$\sin^2\theta$	θ	f(θ)	$\sin^2\theta$
16	.001111	.076	56	.12432	.68730
17	.001411	.0855	57	.13191	.70337
18	.001767	.0955	58	.13976	.71919
19	.002186	.106	59	.14788	.73474
20	.002673	.117	60	.15625	.75
21	.003235	.1284	61	.16488	.76496
22	.00388	.14033	62	.17376	.77960
23	.004614	.15267	63	.1829	.79389
24	.005444	.16543	64	.19228	.80783
25	.006378	.17861	65	.20191	.82139
26	.007423	.19217	66	.21177	.83456
27	.008586	.20611	67	.22186	.8473
28	.009875	.2204	68	.23219	.8597
29	.011297	.23504	69	.24273	.8716
30	.012861	.25	70	.25349	.883
31	.014572	.26526	71	.26445	.894
32	.01644	.28081	72	.27561	.9045
33	.01847	.2966	73	.28697	.9145
34	.02067	.3127	74	.29851	.924
35	.02305	.32899	75	.31022	.933
36	.02561	.3455	76	.3221	.9415
37	.02837	.36218	77	.33413	.9494
38	.031323	.379	78	.34631	.9568
39	.034481	.396	79	.35863	.9636
40	.03785	.4132	80	.37107	.9698
41	.041436	.43041	81	.38363	.9755
42	.04524	.4477	82	.39629	.9806
43	.04928	.4651	83	.40905	.9851
44	.05355	.4826	84	.42189	.9891
45	.058058	.50	85	.4348	.9924
46	.0628	.51745	86	.44777	.9951
47	.067804	.53488	87	.46078	.99726
48	.07305	.5523	88	.47384	.99878
49	.07855	.56959	89	.48691	.9997
50	.0843	.5868	90	.5	1
51	.09032	.60396			
52	.0966	.62096			
53	.10313	.6378			
54	.1099	.6545			
55	.11699	.67101			

TABLE VI SOLIDIFICATION MODEL GRAIN SIZE/MORPHOLOGY PREDICTION

$$y = .75y_{Fe} + .25y_{Ni}$$

Material: Fe - .25 Ni alloy

Wetting Angle: $\theta = 81°$

ΔT °K	v_g/v_n	ℓ cm	$v_{dendrite}$ cm^3	V/N cm^3
148.0	26.1	1.78	5.1×10^{-19}	5.68
149.0	21.7	1.45	4.2×10^{-19}	3.04
150.0	18.0	1.18	3.5×10^{-19}	1.65
153.4	9.95	0.61	1.9×10^{-19}	.22
156.0	6.5	.376	1.2×10^{-19}	5.3×10^{-2}
158.0	4.7	.26	0.9×10^{-19}	1.8×10^{-2}
160.0	3.5	.19	6.8×10^{-20}	6.6×10^{-3}
162.5	2.45	.125	4.9×10^{-20}	1.9×10^{-3}
165.0	1.74	.084	3.75×10^{-20}	6.0×10^{-4}
167.5	1.26	.058	2.95×10^{-20}	2.0×10^{-4}
170.0	.92	.041	2.4×10^{-20}	6.7×10^{-5}
172.5	.686	.03	2.0×10^{-20}	2.4×10^{-5}
175.0	.517	.021	1.7×10^{-20}	9.0×10^{-6}
177.5	.395	.015	1.5×10^{-20}	3.5×10^{-6}
180.0	.306	.011	1.4×10^{-20}	1.4×10^{-6}
182.0	.25	.009	1.3×10^{-20}	0.7×10^{-6}
184.0	.21	.007	1.2×10^{-20}	3.6×10^{-7}
186.0	.17	.006	1.1×10^{-20}	1.9×10^{-7}
188.0	.14	.005	1.06×10^{-20}	1.0×10^{-7}
190.0	.122	.0038	1.01×10^{-20}	0.5×10^{-7}
192.0	.10	.0031	9.6×10^{-21}	3.0×10^{-8}
194.0	.088	.0026	9.2×10^{-21}	1.7×10^{-8}
196.0	.076	.0021	8.8×10^{-21}	9.6×10^{-9}
198.0	.065	.0018	8.4×10^{-21}	5.6×10^{-9}
200.0	.057	.0015	8.1×10^{-21}	3.3×10^{-9}

2.3.3 (Continued)

In Figure 17, the theoretical prediction for morphology parameter is plotted beside a schematic representation of Kattamis and Flemings' findings. The general shape of the experimental curve is assumed to be similar to the theoretical, with a discontinuous change of $v_g/v_n > 1$ to $v_g/v_n < 1$ at $\Delta T = 170°K$. To be consistent with Kattamis and Flemings' results, the experimental curve must also remain less than $v_g/v_n \approx 10$ in the interval $30°K < \Delta T < 170°K$, as is indicated by the onset of asymtotic behavior at about $\Delta T = 154°K$ in Figure 17. In Figure 18, the theoretical and experimental curves for dendrite spacing (or grain diameter) are compared. Although the shapes of the curves are similar, there is a drastic discrepancy between the undercooling scales of the two graphs.

The discrepancies found between the theoretically predicted morphological behavior of Fe-.25Ni alloy during solidification and that which is observed experimentally can be attributed to the simplifying assumptions made to derive the solidification model in its present form, and to the almost complete lack of data for the properties of alloy melts. The facts that v_g/v_n does show a transition from greater than one to less than one at 170°K, albeit a continuous transition, and that the theoretical and experimental curves for dendrite spacing are qualitatively similar, provide grounds for hope that an accurate predictive model for alloy solidification behavior (as a function of ΔT and θ) could be developed with sufficient effort. The failure of the present model to show the proper asymtotic and discontinuous behavior of the morphology parameter, and its failure to match the experimental values of dendrite spacing (except in the region near $\Delta T = 180°K$) provide an indication of how much more effort is needed. The usefulness of a successful and accurate model for predicting solid properties will be discussed in the next Section.

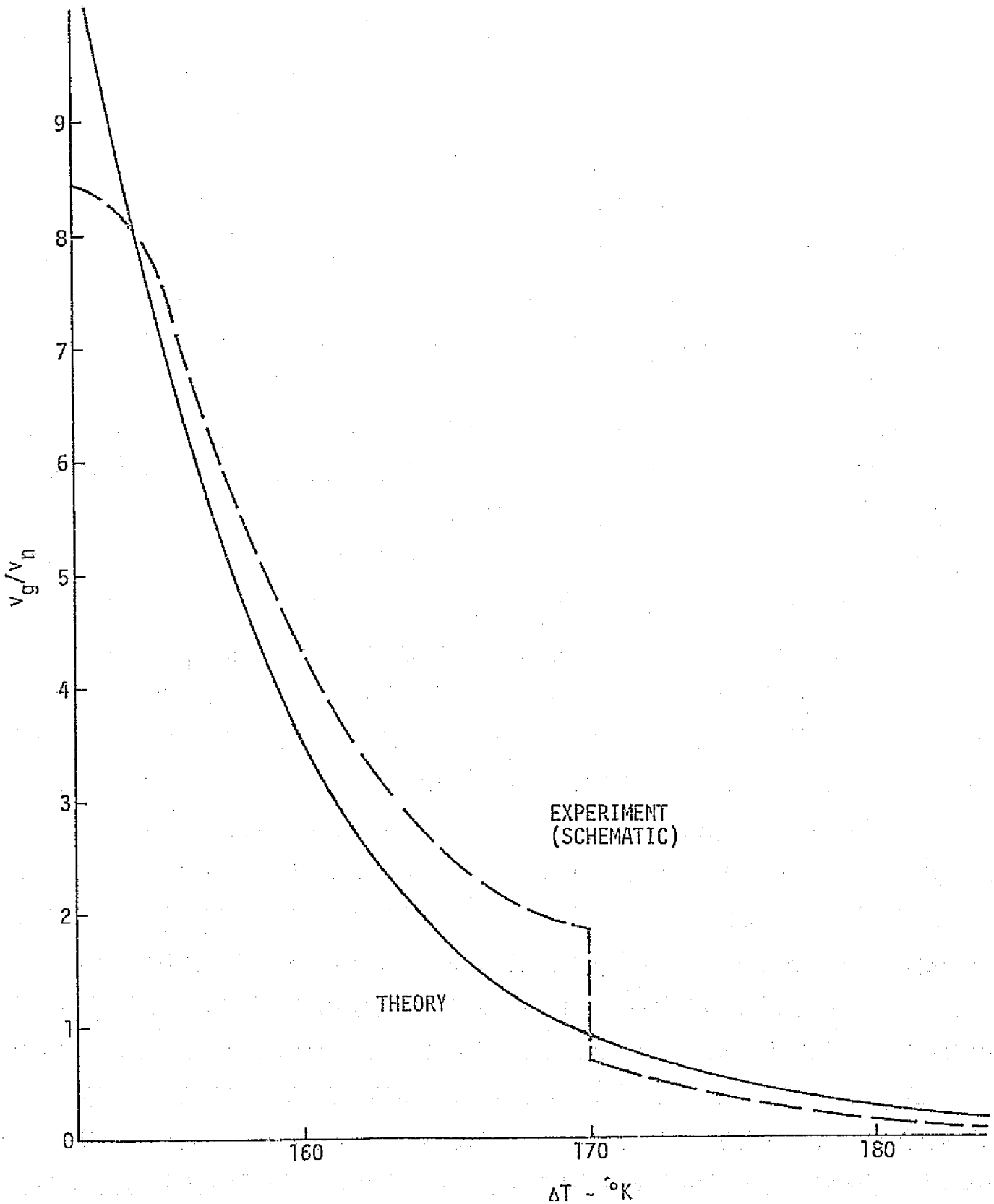

FIGURE 17 MORPHOLOGY PARAMETER VS. UNDERCOOLING FOR Fe-.25 Ni ALLOY, $\theta = 81°$

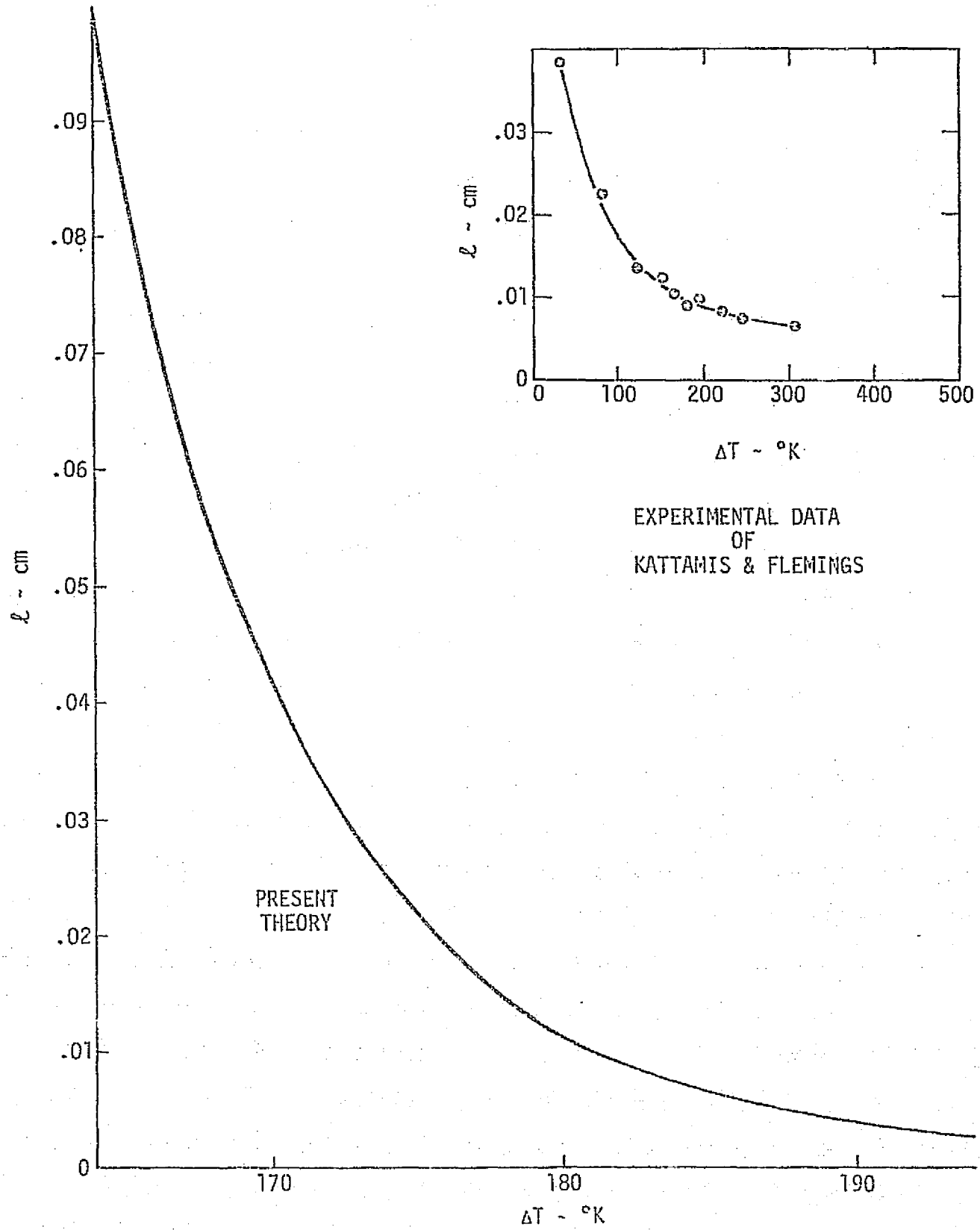

FIGURE 18 DENDRITE ELEMENT SPACING VS. UNDERCOOLING FOR Fe-.25 Ni ALLOY, $\theta = 81°$

2.4 CORRELATION OF THEORY WITH EXPERIMENT

2.4.1 Recommended Procedures and Model Development

Many procedures for the correlation of theory with experiment have been illustrated, if not explicitly stated, in Sections 2.2 and 2.3. The basic problem is to express theory in a manner which predicts the value of parameters which are experimentally measured as a function of parameters which are experimentally controlled. This usually results in the construction of a mathematical model, which, if the theory is sufficiently general, can predict the outcome of a given experiment - values of several parameters - as a function of those constant and variable parameters which characterize the experimental conditions. A good example of this procedure is the definition of the dendrite morphology parameter in Section 2.2.7 and its calculation in Section 2.3.3. Actual comparison with experimental data is often best accomplished with graphical techniques, though other methods such as tables, diagrams or theoretical versus empirical equations may be more informative in specific instances.

Specific procedures will depend on the type of experiment to be performed and the nature of the theory applicable to the experiment. These will be defined by the overall purpose of the work. In the discipline of Solidification in Space, the purpose of theory and experiment should be to build a foundation for the creation of new and/or superior materials in the weightless environment of space, which will meet the requirements of the material user for certain specified properties possessed by the material. A methodology for achieving this purpose is illustrated in Figure 19, which could be considered a logic diagram for a comprehensive material property prediction model, showing how user requirements can be matched to material properties by varying the input parameters which consist of the characteristics of the melt and its external environment - the solidification process controls. Although this diagram indicates a trial-and-error approach to selecting the proper melt components

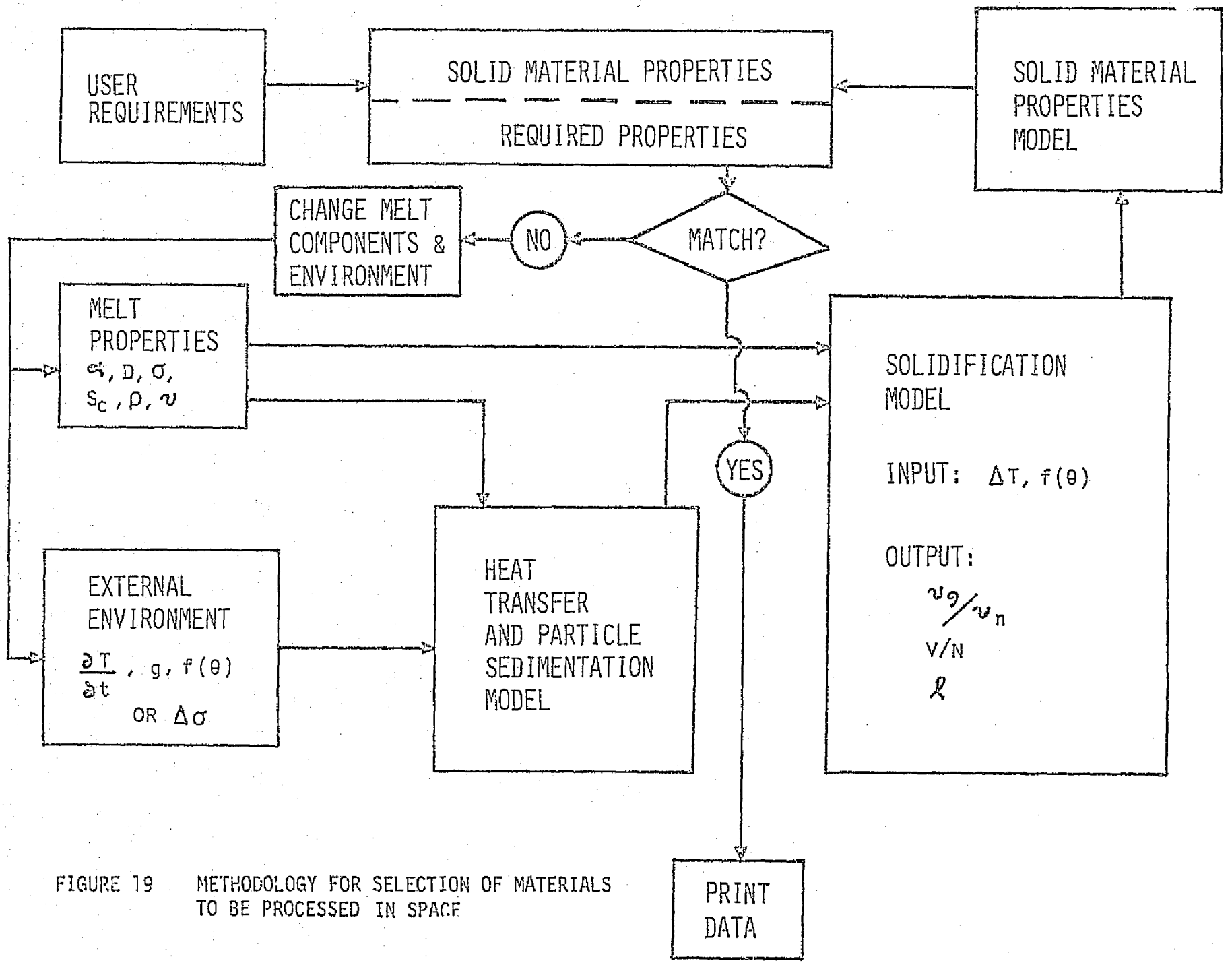

FIGURE 19 METHODOLOGY FOR SELECTION OF MATERIALS TO BE PROCESSED IN SPACE

2.4.1 (Continued)

and environment, it is orders-of-magnitude cheaper to do this analytically than experimentally. There also exists the possibility that as the model matures, methods will be devised to compute required melt components and environment directly from the user requirements without the need for trial-and-error.

In addition to serving as a basic materials design tool, such a comprehensive property prediction model would be invaluable to the Space Processing Program as an aid in selecting those materials for flight experiments which are most likely to produce unique or interesting properties in the space-processed material. Since more than half of the 92 natural elements are used as primary metals or as alloying elements, the number of possible new materials (binary, ternary, quarternary and quinary) is greater than 100 million. Therefore a detailed and rapid method of selecting materials and concentration combinations of potential interest is needed.

The comprehensive property prediction model represented by Figure 19 is composed of several elements, one of which is the solidification model described in Section 2.2.7. Development of each element of the comprehensive model will generate a number of verification experiments, in both one-g and zero-g, to confirm that model predictions correspond to nature, particularly that part of nature which is so removed from everyday experience: zero-g. The concept of a comprehensive material property prediction model is relatively new, and at present only the solidification model mentioned above and the melt property input for the Fe-Ni and Pb-Sn systems have received much attention. But from these, certain procedures for correlating theory with experiment can be ascertained.

The primary factor in determining what materials are to be used in the comparison of theory with experiment is knowledge of the melt properties of the chosen material. If such properties as thermal diffusivity, entropy of fusion, liquid-solid interfacial energy, diffusion coefficient

2.4.1 (Continued)

and density are not known, then the input constants for the solidification model cannot be specified, and nothing can be calculated for the material. Hence, those materials for which melt property values are known should be prime candidates for experiment. Other factors, such as the benefit of a large density differential in the Pb-Sn system, must also be considered in the material selection process.

After selection of materials and definition of the input variables and constants, the quantities to be measured experimentally and predicted theoretically must be determined. Then building of the mathematical model and design of the experiment may proceed. If the experiment has already been performed, as in the case of the Fe-.25 Ni morphology study in one-g, then the quantities to be predicted are specified by the experiment. If the experiment has not been designed, then theory will provide a guide as to what quantities are most desirable or practicable to measure. After performing the experiment, making measurements and carrying out computations with the model, the data obtained should be compared by plotting it on the same graph, displaying it in the same table, etc. In this way the accuracy of the theory in predicting or explaining physical reality can be determined. More specific discussion of comparison procedures and experiment objectives will be given in the following Sections. It is recommended that NASA begin, as soon as possible, to develop a comprehensive material property prediction model, similar to that illustrated by Figure 19, to serve as a theoretical guide for Space Processing development, and later as a molecular-level materials design tool.

2.4.2 Recommendations of Materials for Flight Experiments

As mentioned above, a primary consideration in selecting a material system for study is the availability of data for the liquid state properties of the material. Even when data exists for a material, it may be very difficult to obtain in a form useful for solidification

2.4.2 (Continued)

calculations. A case in point is thermal diffusivity, α_T. Usually thermal diffusivity values are not reported in the literature for liquids, and α_T must be calculated from its defining equation

$$\alpha_T = \frac{\kappa}{\rho\, c_p} \tag{117}$$

where κ is thermal conductivity and c_p is specific heat. The melt values of κ, ρ and c_p must now be obtained. Values of ρ and c_p for liquid elements are fairly common, but κ must often be calculated from electrical conductivity, σ_e, data via the Wiedman-Franz law

$$\kappa = \frac{\pi^2 k^2 T}{3e^2}\, \sigma_e \tag{118}$$

where e is the electron charge.

In addition to the almost complete lack of experimentally determined values for the properties of multi-component melts, there is a dearth of techniques for calculating melt property values for alloys. When all else fails, the simple relation

$$y_{melt} = X\, y_A + (1-X)\, y_B \tag{119}$$

where X is the solute atomic fraction and y_i is the melt value of property y for component i, may be used to obtain an order-of-magnitude estimate for the property y_{melt}. However, with certain exceptions [59], there is no rigorous basis for using equation 119 to obtain alloy melt properties. Other criteria for selecting a material system for theoretical and experimental study include:

- Availability of one-g experiment data bank,
- The practical or scientific importance of the material system,
- The properties of the material system enhance a particular measurement to be made, e.g., different component densities enhance segregation measurement,

C 2

2.4.2 (Continued)

0 Simplicity of the material system with reference to experiment design and theoretical analysis.

Taking these criteria into account, the two material systems recommended for further study, particularly zero-g experimentation, are iron-nickel and lead-tin. Melt property data for the elemental components of these systems is given in Table VII, along with solute diffusion coefficients. Alloy melting temperatures are given by phase diagrams, the atomic weight, density and specific volume can be found by equation 119, and the remaining alloy properties are unknown.

2.4.3 Recommended Experiment Objectives

The primary purpose of the study described by this report has been to define theoretically how undercooling, gravity and nucleants (impurities, high temperature phases or container surfaces) affect the solidification of materials and the resultant solid properties. Hence it is recommended that zero-g experiments (with one-g controls) be designed which will determine the effects of these environmental variables on solidification and solid properties. Several specific experiment types can be identified:

Segregation Experiments

These experiments would essentially repeat the MSFC centrifuge experiments with Pb-Sn eutectic melts, but be performed in zero-g to isolate the unexplained undercooling effect on solute segregation from the gravity effects. Volume fraction (or atomic fraction) of lead and temperature (undercooling) would be the primary variables measured.

Morphology Experiments

Morphology experiments would be designed to measure nucleation rate, growth rate, grain size and dendrite morphology as functions of undercooling and nucleant wetting angle (or other parameter appropriate to characterization of the nucleant). The undercooling and rate measurements

TABLE VII LIQUID STATE/SOLIDIFICATION PARAMETERS FOR SELECTED MATERIALS

ELEMENT	T_m °K	M gm/gm atom	ρ gm/cm^3	v cm^3/gm atom	σ ergs/cm^2	S_c ergs/cm^3°K	K watt/°K cm	C_p joule/gm°K	α_T cm^2/sec
Fe	1809	55.85	6.9	8.09	204	$12X10^6$	0.39	0.7866	0.072
Ni	1725	58.71	8.0	7.34	255	$15.5X10^6$	0.469	0.6556	0.089
Pb	600.6	207.21	10.3	20.1	33.3	$4.34X10^6$	0.165	0.1417	0.106
Sn	505	118.7	6.98	17.0	59	$8.53X10^6$	0.369	0.2590	0.216
REFERENCES	PERIODIC TABLE	PERIODIC TABLE	INT. CRIT. TABLES	M/ρ	D. TURNBULL		INT. CRIT. TABLES	HULTGREN, et. al.	K/ρC_p

DIFFUSION DATA: $D_{Ni \rightarrow Fe} = 4.67X10^{-5}$ cm^2/sec

$D_{Pb \rightarrow Sn} = 3.69X10^{-5}$ cm^2/sec

2.4.3 (Continued)

would be made during the zero-g flight period of the experiment, and morphological measurements could be made later after sectioning the sample. In making morphological measurements, a method should be devised for measuring the average size or volume of the dendrites. From the dendrite volume, v_d, the morphology parameter may be obtained directly by

$$v_g/v_n = v_d/v_n - 1 \tag{120}$$

where the nucleus volume, v_n, is obtained from the undercooling and wetting angle by equation 95.

Undercooling and Nucleation Experiments

The purpose of these experiments would be to determine the effects of gravity and nucleants, including container surfaces, on melt undercooling. Of particular interest are convection effects on undercooling (temperature) distribution in the melt and the influence this distribution has on nucleus formation and growth-especially on interface stability. A goal of containerless solidification experiments in zero-g, is to establish the importance of container surfaces as nucleants which limit the achievable undercooling, and thus, control over solid properties. The control experiment in this case would be another zero-g sample which is in a container. In all cases the measurement required will be undercooling (temperature) as a function of position in the melt. Additional measurements of convective heat transfer and g level will be desirable in the gravity-dependent experiments.

Nucleant Characterization Experiments

These experiments will attempt to specify the most convenient parameter for characterizing the influence which nucleant interfacial energies have on the nucleation and growth processes. Parameters used in this report include nucleus-melt interfacial energy, $\sigma_{n\ell}$ or σ, θ (equation 16) and $\Delta\sigma$ (equations 21). If, for example, it is found that most nuclei

2.4.3 (Continued)

which form are of the spherical cap type, a further purpose of these experiments would be to correlate θ values with particular impurity (nucleant) - melt combinations and to hopefully provide insight into the mechanism which causes a nucleus to form more readily on one type of nucleant than on another. If this insight is obtained, it should provide some understanding of denucleation as well.

Melt Property Measurements

As mentioned previously, the main problem encountered in the calculation of theoretical predictions of solidification phenomena (disregarding the accuracy of the theory itself), is the dearth of values for the properties of the melt which usually appear as constants in the equations of the theory. Since most of these properties are defined as fundamental constants for the material or are derived from intermolecular structure and energy in a formal manner which can not yet be reduced to numerical calculation, experimental measurement of these properties is the most direct method for obtaining them. This is usually quite difficult for metals and alloys due to the high temperatures required by the liquid state and the sometimes corrosive nature of the metal melt being studied. But if the ability to predict the results of solidification processes and to enter an era of true design of material properties at the molecular level is to be attained, values of melt properties such as thermal diffusivity, interfacial energy (or a corresponding parameter), diffusion coefficient, specific volume (density), isothermal compressibility, thermal expansion coefficient and entropy of fusion must be obtained.

2.5 REFERENCES

1. R. Becker and W. Döring, Ann. d. Physik [5] 24, 719, 1935.

2. R. Becker, Ann. Physik, 32, 128, 1938.

3. D. Turnbull and J. C. Fisher, J. Chem. Phys., 17, 71, 1949.

4. D. Turnbull, J. Appl. Phys., 21, 1022, 1950.

5. J. H. Hollomon and D. Turnbull, in Progress in Metal Physics (B. Chalmers and R. King, eds.) Vol. 4, pp 333-388, Pergamon, London, 1953.

6. See for further references, K. A. Van Wormer, Jr., A Review Study of Nucleation and Its Role in Solidification, AMMRC CR 69-08, Army Materials and Mechanics Research Center, Watertown, Mass., 1969.

7. D. Turnbull, Trans. Met. Soc. AIME, 221, 422, 1961.

8. J. Lothe and G. M. Pound, in Nucleation (A. C. Zettlemoyer, ed.) pp 109-150, Marcel Dekker, New York, 1969.

9. W. J. Dunning, in Nucleation (A. C. Zettlemoyer, ed.) pp 1-68, Marcel Dekker, New York, 1969.

10. F. L. Binsbergen, in Progress in Solid State Chemistry (J. O. McCaldin and G. Somorjai, eds.) Vol. 8, pp 189-238, Pergamon, London, 1973.

11. D. P. Moak, N. M. Griesenauer and S. H. Gelles, Final Report on Contract NAS8-28749, Battelle Columbus Labs, April 18, 1975.

12. D. Turnbull and B. Vonnegut, Ind. Eng. Chem., 44, 1292, 1952.

13. B. E. Sundquist and L. F. Mondolfo, Trans. Met. Soc.-AIME, 221, 607, 1961.

2.5 (Continued)

14. M. E. Glicksman and W. J. Childs, Acta Met., 10, 925, 1962.

15. A. G. Walton, in Nucleation (A. C. Zettlemoyer, ed.) pp 225-308, Marcel Dekker, New York, 1969.

16. G. F. Davies, Solidification and Casting, John Wiley & Sons, Inc., New York, 1973.

17. W. C. Winegard, An Introduction to the Solidification of Metals, The Institute of Metals, London, 1964.

18. R. I. Miller and R. C. Ruff, J. Appl. Phys., 46, 208, 1975.

19. S. Toschev, Crystal Growth, An Introduction, (P. Hartman, ed.), pp 1-49, North-Holland Publishing Co., Amsterdam, 1973.

20. K. A. Jackson, Nucleation Phenomena, (A. S. Michaels, ed.), pp 37-40, American Chemical Society, Washington, 1966.

21. D. Turnbull and M. H. Cohen, Modern Aspects of the Vitreous State, (J. D. Mackenzie, ed.), pp 38-62, Butterworths, Washington, 1960.

22. W. B. Hillig and D. Turnbull, J. Chem. Phys., 24, 914, 1956.

23. D. Turnbull and R. E. Cech, J. Appl. Phys., 21, 804, 1950.

24. D. Turnbull, J. Metals, 188, 1144, 1950.

25. D. Turnbull, Scientific American, 212, 38, 1965.

26. W. V. Youdelis and S. P. Iyer, J. Inst. Metals, 101, 176, 1973.

27. S. P. Iyer and W. V. Youdelis, J. Inst. Metals, 100, 372, 1972.

28. S. Y. Shiraishi and R. G. Ward, Can. Met. Quart., 3, 117, 1961.

29. M. E. Glicksman and C. L. Vold, Acta Met., 17, 1, 1969.

2.5 (Continued)

30. K. Huang, Statistical Mechanics, pp 157,158, John Wiley & Sons, Inc., New York, 1967.

31. H. Eyring, D. Henderson, B. J. Stover and E. M. Eyring, Statistical Mechanics and Dynamics, p 369, John Wiley & Sons, Inc., New York, 1964.

32. R. I. Miller, A Summary of Liquid State Models for Materials Processing in Space, Boeing Document D5-17268 (unpublished).

33. K. Huang, ibid, p 259.

34. F. Spaepen, Acta Met., 23, 729, 1975.

35. J. D. Bernal, Nature, Lond., 185, 68, 1960.

36. J. D. Bernal, Proc. Roy. Soc., A280, 299, 1964.

37. J. L. Finney, Proc. Roy. Soc., A319, 479, 1970.

38. A. S. Skapski, Acta Met., 4, 576, 1956.

39. D. Turnbull, Liquids: Structure, Properties, Solid Interactions, (T. J. Hughel, ed.) pp 14-16, Elsevier Publishing Co., New York, 1965.

40. C. Herring, The Physics of Powder Metallurgy, (W. E. Kingston, ed.), pp 143-178, McGraw-Hill, New York, 1951.

41. I. A. Kotźe and D. Kuhlmann-Wilsdorf, Appl. Phys. Lett., 9, 96, 1966.

42. D. Kuhlmann-Wilsdorf, Phys. Rev., 140, A1599, 1965.

43. W. T. Read and W. Shockley, Phys. Rev., 78, 275, 1950.

44. H. B. Huntington, Solid State Physics, vol. 7, (F. Seitz and D. Turnbull, eds.), pp 214-352, Academic Press, Inc., New York, 1958.

2.5 (Continued)

45. A. Cibula, J. Inst. Metals, 76, 321, 1949.

46. J. J. Burton, Acta Met., 21, 1225, 1973.

47. A. Moore and R. Elliott, in The Solidification of Metals, ISI Publication 110, pp 167-172, The Iron and Steel Institute, London, 1967.

48. B. Chalmers, Principles of Solidification, John Wiley & Sons, New York, 1964.

49. D. Turnbull and M. H. Cohen, J. Chem. Phys., 34, 120, 1961.

50. W. W. Mullins and R. F. Sekerka, J. Appl. Phys., 35, 444, 1964.

51. R. F. Sekerka, J. Appl. Phys., 36, 264, 1965.

52. R. I. Miller and W. S. Chen, Further Analysis of Field Effects on Liquids and Solidification, NASA CR-120313, Boeing Aerospace Company, July, 1974.

53. R. F. Sekerka, J. Phys. Chem. Solids, 28, 983, 1967.

54. J. M. Ziman, Principles of the Theory of Solids, Cambridge University Press, Ch. 7, 1964.

55. J. M. Ziman, Electrons and Phonons, Oxford Press, Ch. 8, 1960.

56. T. Z. Kattamis and M. C. Flemings, Trans. Met. Soc., AIME, 236, 1523, 1966.

57. M. H. Johnston and C. S. Griner, Scripta Met., (to be published).

58. T. E. Strangman and T. Z. Kattamis, Met. Trans., 4, 2219, 1973.

59. R. Hultgren, R. L. Orr, P. D. Anderson and K. K. Kelley, Thermodynamic Properties of Metals and Alloys, John Wiley & Sons, Inc., New York, 1963.